TU Delft

Delft University of Technology

Document Version
Final published version

Licence
CC BY

Citation (APA)
Frem, M. R., Stigter, T. Y., van Breukelen, B. M., Gettel, G. M., Jewitt, G. P. W., & Mwakachola, B. (2026). Building a data-driven conceptual model of the hydrological functioning of the Taita Hills tropical water tower system in Kenya. *Journal of Hydrology*, *681*, Article 136595. https://doi.org/10.1016/j.jhydrol.2026.136595

Important note
To cite this publication, please use the final published version (if applicable).
Please check the document version above.

Copyright
In case the licence states “Dutch Copyright Act (Article 25fa)”, this publication was made available Green Open Access via the TU Delft Institutional Repository pursuant to Dutch Copyright Act (Article 25fa, the Taverne amendment). This provision does not affect copyright ownership.
Unless copyright is transferred by contract or statute, it remains with the copyright holder.

Sharing and reuse
Other than for strictly personal use, it is not permitted to download, forward or distribute the text or part of it, without the consent of the author(s) and/or copyright holder(s), unless the work is under an open content license such as Creative Commons.

Takedown policy
Please contact us and provide details if you believe this document breaches copyrights.
We will remove access to the work immediately and investigate your claim.

This work is downloaded from Delft University of Technology.

Journal of Hydrology 681 (2026) 136595

Contents lists available at ScienceDirect

Journal of Hydrology

journal homepage: www.elsevier.com/locate/jhydrol

Research papers

Building a data-driven conceptual model of the hydrological functioning of the Taita Hills tropical water tower system in Kenya

Michel R. Frem [a,b,*], Tibor Y. Stigter [a], Boris M. van Breukelen [b], Gretchen M. Gettel [a,c], Graham P.W. Jewitt [a,b], Benson Mwakachola [d]

[a] IHE Delft Institute for Water Education, Water Resources and Ecosystems Department, The Netherlands
[b] Delft University of Technology, Department of Water Management, The Netherlands
[c] Aarhus University, Department of Ecoscience – Freshwater Ecology, Denmark
[d] Independent Water Expert, Kenya

ARTICLE INFO

This manuscript was handled by Dongmei Han, Editor-in-Chief

Keywords:
Water towers
Hard-rock aquifers
Tropical mountain hydrology
Chloride mass balance
Tritium
Baseflow

ABSTRACT

Tropical natural water towers regulate downstream freshwater resources, yet their hydro(geo)logical functioning remains poorly understood. This study integrates multi-year (2022-2025), multi-season hydroclimatic and tracer observations to build a data-driven conceptual model of a tropical metamorphic water tower at Taita Hills in Kenya. The collected dataset enabled rainfall partitioning, baseflow separation, multiple-method recharge estimations, hydrochemical and tritium analyses, and various spatial and multivariable analyses. Results show that the highland subcatchments, representing 43% of the catchment area, account for 87% of total discharge. Actual recharge is approximately twice as high in the highlands as in lower subcatchments. At the subcatchment scale, recharge ratios in more forested and elevated subcatchments (25% of rainfall) are about 1.5 times higher than in thicket-dominated subcatchments. The perennial behavior of most springs and streams, and the high baseflow contribution, indicate an important groundwater-buffering capacity. Evidence suggests that structural geology influences subsurface flow between subcatchments and baseflow in the streams. Spatial variations in lateral subsurface flow, higher specific discharge, and higher spring density in the south point towards cross-subcatchment transfers facilitated by lineaments. Hydrochemical and isotope analyses indicate increasing mineralization and (yearly to decadal) residence times from highlands to lowlands. These results indicate highland-lowland connectivity and show that the Taita Hills function as a groundwater-dominated water tower, where highlands are the main precipitation input zones, storage capacity is large, and preferential flow pathways sustain downstream and dry-season flows. More broadly, these findings reinforce the need to account for subsurface processes when assessing the hydrology of water towers.

1. Introduction

Mountains are home to about 1.1 billion people and contribute up to 60% of total freshwater resources (UN, 2025). In recent years, mountains have received increasing global attention, particularly through the UN World Water Development Report 2025, which focused on mountains and glaciers as the world's natural water towers. Together with adjacent low-lying terrains, water towers form complex highland-lowland systems (Messerli, 1983; Messerli et al., 1988). Understanding these systems requires identifying how water is stored, transferred, and released across the highland-lowland gradient.

Due to their higher elevations, water towers receive significant orographic precipitation (e.g., Immerzeel et al., 2020), thereby supporting their function as major zones of precipitation input. This function is manifested by a disproportionate contribution from mountain areas to total runoff (Messerli et al., 2004; Viviroli et al., 2007). In extreme cases, mountain discharge may account for up to 95% of the total flow in some catchments (Liniger et al., 1998). Natural water towers are also characterized by their groundwater storage and streamflow regulation functions, which support reliable water supply (Messerli et al., 2004) and consequently sustain both ecological and anthropogenic water demands downstream (Immerzeel et al., 2020). In these systems, streamflow is often dominated by groundwater contributions, especially in relatively undisturbed systems (Bruijnzeel, 2004).

* Corresponding author at: Delft, South Holland, The Netherlands.
E-mail address: m.frem@un-ihe.org (M.R. Frem).

https://doi.org/10.1016/j.jhydrol.2026.136595
Received 29 May 2026; Received in revised form 7 October 2026; Accepted 9 October 2026
Available online 14 October 2026
0022-1694/© 2026 The Author(s). Published by Elsevier B.V. This is an open access article under the CC BY license (http://creativecommons.org/licenses/by/4.0/).

However, many global water-tower assessments have focused specifically on cryospheric systems, where the buffering function is supported by snow and glacier storage and delayed melt processes (Immerzeel et al., 2020); in non-cryospheric water tower systems, this buffering function is generally provided by other forms of storage and hydrological processes. Somers and McKenzie (2020) have highlighted the importance of groundwater across many mountain systems, particularly during low-flow periods.

The most critical water towers are located in dry climate zones (Messerli et al., 2004), where the semi-arid lowlands are highly dependent on discharge and baseflow from the humid highlands. This is particularly evident in Africa, which hosts approximately 11% of the global mountain area (Alweny et al., 2014). Despite their importance, the hydrological behavior of tropical and subtropical mountains remains insufficiently understood (Bruijnzeel, 2001; Viviroli et al., 2003), largely due to the complexity of such hard-rock systems, limitations in data availability (Hughes et al., 2015) and field accessibility (Messerli et al., 1988). Building this knowledge is increasingly critical with highland migration, land use change and climate change placing immense pressure on locally available water resources. Rainfall and water flows originating from the highlands are becoming more erratic, with shifts in the timing and magnitude of both peak and low flows (Barnett et al., 2008; Adler et al., 2022; UN, 2025). During periods of drought, groundwater resources become particularly important (Palmer et al., 2023), as they sustain domestic and agricultural water needs (Ferrer et al., 2019; Adloff et al., 2022).

Consequently, the spatiotemporal assessment of groundwater recharge, subsurface transfer and mountain discharge based on field data is essential (Harris et al., 2010; van Wyk et al., 2012; Waswa et al., 2013; Sun et al., 2013), yet remains limited. Existing recharge estimation methods generally represent different spatial and temporal scales and have their specific limitations. Hence, combining various, complementary approaches can improve the reliability of the recharge analysis (Scanlon et al., 2002). Hydrograph separation provides important information on groundwater contributions to streamflow, although results may be sensitive to the applied method and parameterization (Eckhardt, 2012). Environmental tracers and hydrochemical indicators also provide information on groundwater recharge, residence times and flow paths (Hilberg, 2016; Jasechko, 2019). In fractured hard-rock aquifers, weathering profiles and fracture networks strongly influence groundwater storage and flow, making their characterization important for understanding groundwater flow pathways (Lachassagne et al., 2021). Nevertheless, process-oriented studies remain limited, despite their importance for identifying dominant hydrological mechanisms and highland-lowland connectivity in water tower systems under diverse hydroclimatic and geological conditions. Existing studies have focused on the comparative assessment of observed variables (mainly runoff) between highlands and lowlands, with limited analyses and measurements aimed at refining the conceptual model by assessing the underlying processes, particularly those occurring in the transition zone.

Within this context, the Taita Hills region in Kenya was selected for this field-based, data-driven study. The hydrological value of the tropical montane forests of the Taita Hills is significant (Hohenthal et al., 2015), as these forests can provide substantial amounts of water to local ecosystems (Hamilton and Cassells, 2003; Bruijnzeel, 2004) and downstream lowlands. As in many mountainous regions, the removal of indigenous trees has reduced water retention capacity and water availability in the Taita Hills, reflected in drastic declines in spring and stream discharge over the past five decades, as highlighted by local communities (Hohenthal et al., 2015). Early research in the Taita Hills, which cover approximately 400 km^2 (Borghesio et al., 2010), focused on geological mapping (Horkel et al., 1979). Subsequent studies increasingly addressed land cover changes (Clark and Pellikka, 2009; Pellikka et al., 2009; Piiroinen et al., 2015; Abera et al., 2022). Mkaya (2013) and Obando et al. (2024) evaluated the impacts of land cover change on river flows in the Wundanyi catchment, while Hohenthal et al. (2015) assessed changes in water-related ecosystem services in both the Wundanyi and Mwatate catchments. Cardwell (2017) investigated the effects of land cover on infiltration in the Ngangao indigenous forest of the Taita Hills.

More recent studies have focused on groundwater processes, including the mapping and assessment of springs and groundwater flow systems (Khan, 2022), the resilience of springs to drought conditions (Cardozo, 2022), the impacts of land cover change and climate variability on groundwater recharge (Mwende, 2022), and the relationship between groundwater recharge and discharge in the Wundanyi catchment (Etukutan, 2024). While these studies provide valuable insights, they often address individual components of the hydrological cycle with limited temporal coverage and rely on sporadic measurements. This also reflects a wider challenge in water tower research, where integrated analyses remain limited, particularly in tropical environments.

Consequently, the main goal of this study was to conduct an integrated data-driven assessment of the conceptual functioning of a tropical water tower system, including rainfall partitioning, groundwater recharge, the coupling of surface and subsurface processes and the relative roles of seasonality, vegetation type, geology, and topography. The study was based on an extensive multi-season, field-based investigation of the Taita Hills highland-lowland system conducted between 2022 and 2025, focusing primarily on the Wundanyi catchment and, to a lesser extent, the Mwatate catchment. The field investigations focused on collecting a large dataset, including stream level, discharge and chemistry, spring discharge and chemistry, and rainfall rates and chemistry, to study this complex water tower system.

2. Study area

The study area comprises the Wundanyi and Mwatate catchments in the Taita Hills in Kenya, with surface areas of 49.5 and 57.4 km^2, respectively. Topographic elevation within the study area shows strong variability (Fig. 2), ranging from approximately 670 m above mean sea level (AMSL) in the lowlands to 2055 m AMSL at Iyale, the highest peak in the study area. The Taita Hills area has an arid-to-semiarid climate in the lowlands and a tropical savannah climate in the highlands (Kivivuori, 2013). Historical records show that annual rainfall in Mwatate, at the base of the southern footslopes of the study area, is around 600 mm. In contrast, in Wundanyi, situated at an elevation of approximately 1400 m AMSL, annual rainfall reaches about 1329 mm (East African Meteorological Department, 1966). Orographic rains on the eastern and southeastern slopes of the Taita Hills result from moisture generated by the shifting position of the Intertropical Convergence Zone (ITCZ) and the condensation of vapor from the Indian Ocean (Beentje and Ndiang'ui, 1988; Maeda et al., 2011). In contrast, slopes in the rain shadow area receive lower amounts of rainfall than the eastern side (Horkel et al., 1979; Vogt and Wiesenhuetter, 2000). The area experiences a bimodal rainfall distribution, with the long rains typically occurring between March and May and the short rains between October and December. This pattern is largely influenced by the seasonal migration of the ITCZ (Tuhkanen, 1991; Vogt and Wiesenhuetter, 2000). Furthermore, mist and cloud precipitation contribute to overall moisture throughout the year in the mountain forests of the Taita Hills (Beentje and Ndiang'ui, 1988).

The Taita Hills are a Precambrian mountain range located within the Mozambique Belt (Oosterom, 1988) and constitute the northernmost part of the Eastern Arc Mountain range (Cardwell, 2017). The research area mainly consists of the Kasigau and Kurasi groups. The Kasigau group, occurring in the northern part of the Wundanyi catchment (Fig. 1), is characterized by a thick, repetitive sequence of quartz-feldspar gneisses. The Kurasi group, encountered in the central and southern parts of the study area, is more complex and comprises various biotite gneisses with intercalations of marble, sillimanite, kyanite, and graphite gneisses (Horkel et al., 1979). Metamorphic gneiss rocks form the main bedrock unit, while soil units overlying undifferentiated

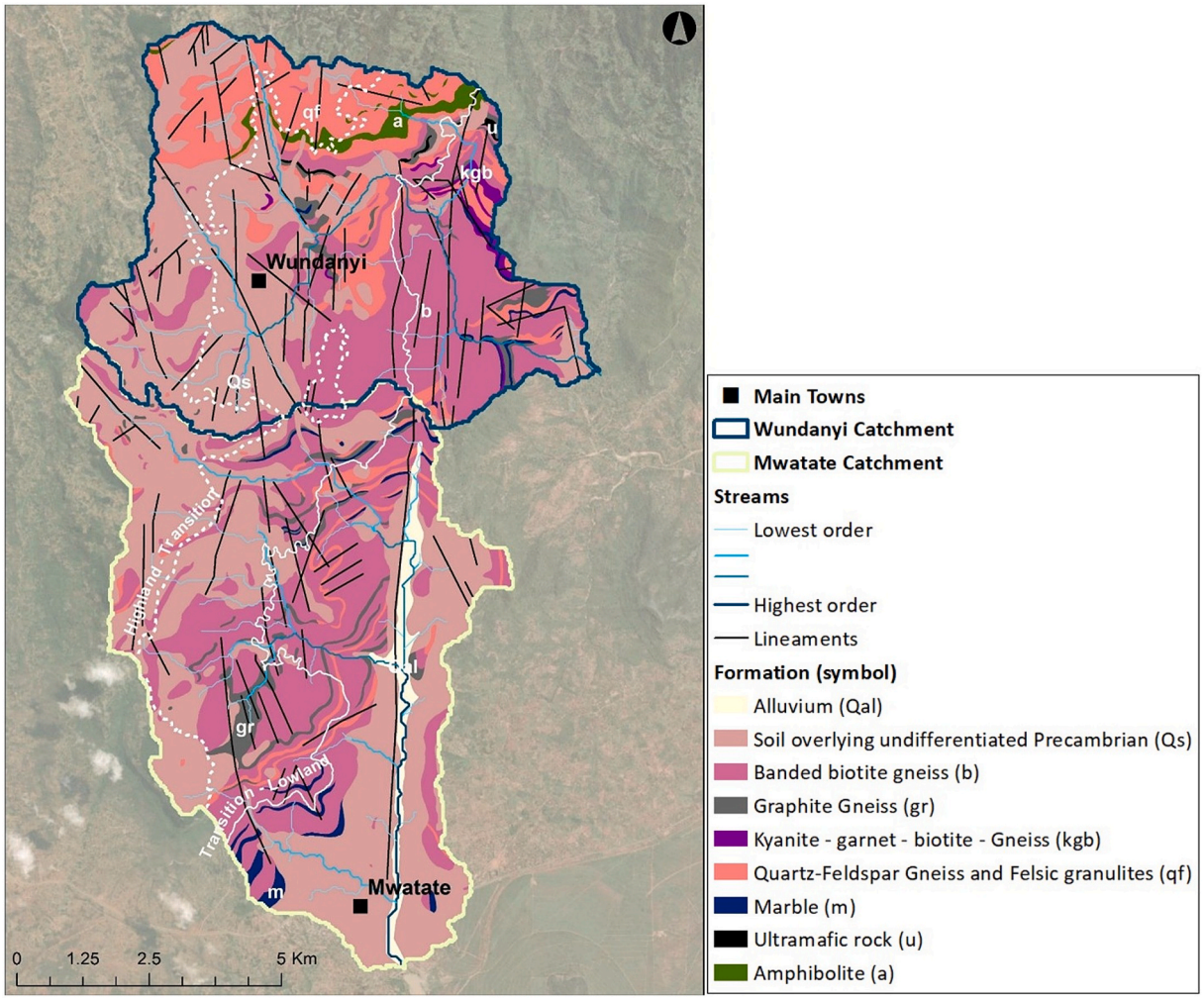


Fig. 1. Geological map of the Wundanyi and Mwatate catchments, modified after Horkel et al. (1979) and Kaistinen et al. (2018). Lineaments were digitized by the authors from the structural geology map of Taita Hills, initially prepared by Horkel et al. (1979).

Precambrian formations cover around 46% of the study area. Occasional outcrops of alluvium, marble, amphibolite, and ultramafic rocks are also present at some locations (see Fig. 1). As a result of weathering of the gneissic bedrock, well-drained and fertile cambisols constitute the dominant soil type in the Taita Hills (MoEaM, 2013). Many lineaments are present in the study area, mainly oriented north-south. North-south lineaments in the Taita Hills were interpreted as extensive tensional structures with no significant vertical displacement (Horkel et al., 1979; Pohl et al., 1980), promoting groundwater flow through the resulting open fractures. Indeed, groundwater in the metamorphic rocks of the southern Taita Hills was reported to occur mainly in fissures, fractures, and fault systems (Pohl and Niedermayr, 1979).

The Wundanyi and Mwatate catchments are relatively small but steep systems (Fig. 2), and therefore often generate rapid runoff responses to rainfall events. Stream orders in the Wundanyi catchment range from first to third order and drain towards Msau. In contrast, the Mwatate catchment has a slightly more developed drainage network, with stream orders reaching fourth order upstream of the outlet. The unconsolidated superficial deposits encountered in the study area form an unconfined aquifer characterized by relatively high permeability and porosity. However, these deposits are generally shallow and of limited spatial extent. Exploitable aquifers in the Taita Hills are mainly deeper, confined systems associated with both the primary and secondary porosity of the metamorphic bedrock. These fractured aquifers commonly discharge in the form of springs (Horkel et al., 1979), which are predominantly contact, fault, and depression springs (Mwende, 2022).

Thicket covers 40% of the study area, followed by agroforestry at 33% and cropland at 14%. Thicket areas feature bushes and climbers up to 7 m tall. In contrast, agroforestry consists of herbaceous crops such as maize and bananas, as well as native and exotic trees, including silky oak, mango, eucalyptus, and Ficus thonningii. Forests cover 8.5% of the study area: montane forests include native tree species reaching heights of 17 to 28 m, while plantation forests consist of exotic eucalyptus, pine, and cypress trees, with average heights of 8 to 29 m. Built-up areas cover less than 1% of the study area. These land cover descriptions have been compiled from various sources (Clark and Pellikka, 2009; Pellikka et al., 2009; Heikinheimo, 2015; Pellikka et al., 2018). Field photographs of different land cover classes are provided in the Supplementary Material.

3. Data and Methods

The adopted research methodology employed an integrated, multi-method field and data analysis approach. Spring mapping was initiated in 2022. Site investigations, conducted between July 2023 and October 2025, included collecting field observations, installing a hydrometeorological monitoring network, measuring spring and stream discharge, and conducting water quality measurements and sampling of rainwater, groundwater, and surface water. Data interpretation comprised climate data analysis, groundwater recharge estimation, baseflow separation, water balance calculations, and water quality analyses, among other analytical approaches. The different lines of

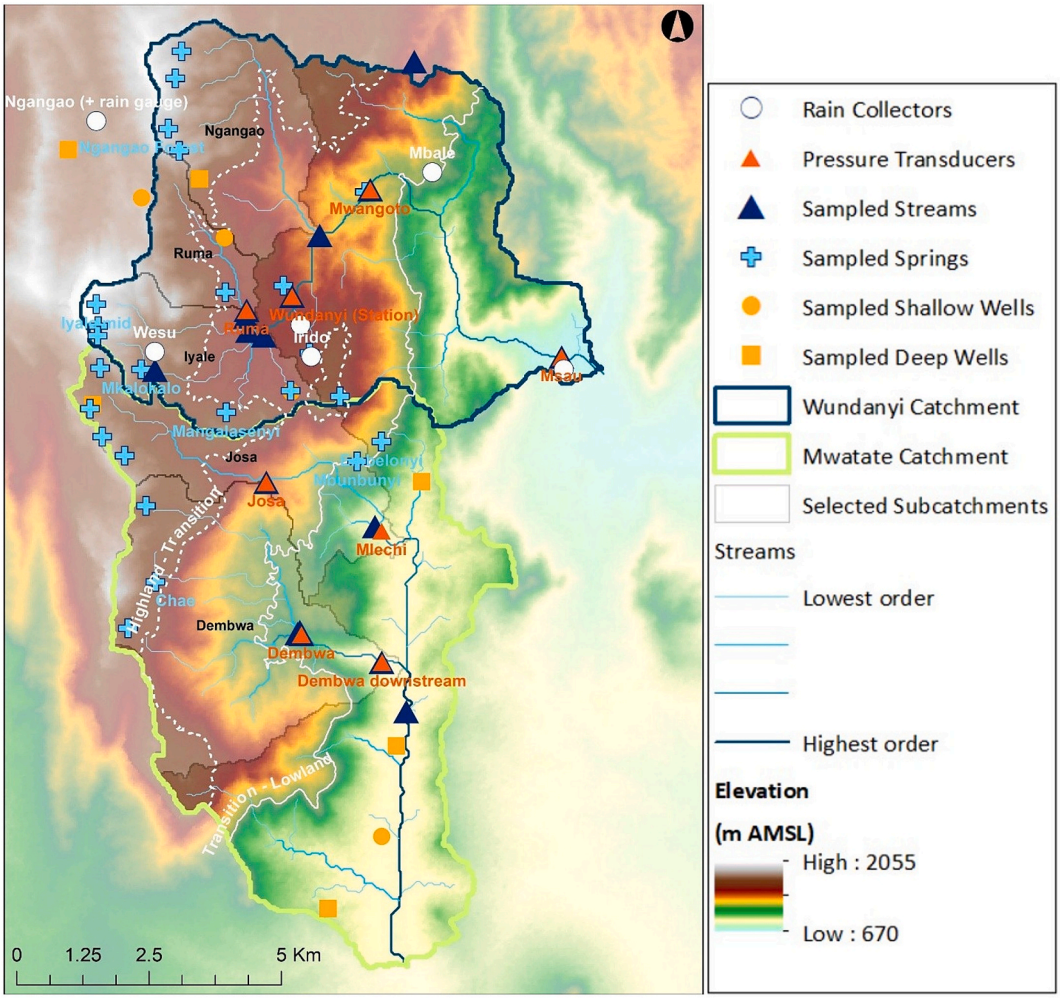


Fig. 2. Sampling locations and monitoring network established in this study. The map also shows topographic elevation, selected subcatchments, and the drainage network, derived from the SRTM 1 arc-second global topographic dataset.

evidence generated through these methods were integrated to develop a data-driven conceptual model of the study area's hydrological functioning. The symbols used in the equations are summarized in Appendix A (Table A.1) along with their meanings and indicative units.

3.1. Hydrometeorological data collection

Hourly rainfall data, provided by the Taita Research Station/University of Helsinki team, were obtained from seven monitoring locations (see Fig. S1). Hourly air temperature values were also provided for the Wundanyi and Kishenyi stations. In April 2024, an additional WTB100 tipping-bucket rain gauge was installed in the Ngangao forest, within the Ngangao Community Resource Center, to capture high-elevation rainfall on the windward side.

Van Essen TD-Diver pressure transducers were installed in eight streams to continuously record water levels (Fig. 2). Monitoring focused on the main Wundanyi River in the Wundanyi catchment, as well as the Josa and Dembwa streams in the Mwatate catchment. Abrupt step changes, including those associated with sensor retrievals, were identified and corrected before further analysis. Atmospheric pressure was monitored using Baro-Diver dataloggers, allowing for barometric compensation of the stream total pressure records. To convert water-level data into discharge, rating curves were developed for each monitored stream (Figs. S2 and S3). For this purpose, stream discharge was primarily measured using an OTT MF Pro electromagnetic flowmeter, which is suitable for low-flow conditions (OTT HydroMet, 2020). Spot, mission-based discharge measurements were conducted across different seasons to capture low-, medium-, and, when field conditions permitted, high-flow conditions. Power-law and polynomial relationships were tested, and the best-fitting function was assigned for each site. The number and range of stage-discharge measurements are summarized in Table S1. At Wundanyi, separate curves were applied before and from 22 December 2023 onwards, because the measurement section and method changed. At Msau, the data showed distinct low-, intermediate-, and high-flow branches; therefore, separate curves were applied accordingly. To assess the effect of extrapolation beyond the gauged range, the maximum stage represented by each calibration dataset was compared with the relevant continuous discharge series. A sensitivity analysis was subsequently performed by varying the discharge estimates associated with stages above the maximum gauged stage by ±30%, as reported in Table S1.

In addition to the continuous stream monitoring, a synoptic low-flow survey was conducted at the outlets of several subcatchments to quantify baseflow at the end of the dry season preceding the long rains. Spring discharge was mainly determined using simple field techniques, including the float method and the volumetric (bucket) method.

3.2. Baseflow separation

Baseflow separation was conducted using daily discharge data at the outlet of the Wundanyi catchment between November 2022 and January 2026, and for four subcatchments, namely Ngangao, Ruma,

Iyale and Dembwa (see Fig. 2 for locations), for the year 2024. This analysis was not performed for other subcatchments because they were not monitored or because the available time series were relatively short. Baseflow separation was performed using the SepHydro tool (Danielescu et al., 2018) by applying graphical techniques, namely the three methods of Pettyjohn and Henning (1979), and a recursive digital filtering technique, namely the method of Eckhardt (2005).

The baseflow hydrograph is determined using the methods of Pettyjohn and Henning (1979), namely the fixed window, sliding window, and local minima approaches, all of which connect low points in the streamflow hydrograph. The window width is defined as 2N and should be the nearest odd integer between 3 and 11. The parameter N represents the duration (in days) of stormflow following a storm event and is empirically related to the drainage area A (expressed in square miles) as $N = A^{0.2}$. Accordingly, the adopted interval width is 3.

The approach of Eckhardt (2005) is based on the concept of a digital filter that decomposes the hydrograph into low-frequency (baseflow) and high-frequency (stormflow) components:

$$Q_{b,i} = \frac{(1 - BFI_{max}).\alpha.Q_{b,i-1} + (1 - \alpha).BFI_{max}.Q_{t,i}}{1 - \alpha.BFI_{max}} \quad (1)$$

Where:

$Q_{b,i}$= baseflow at timestep i [L^3T^{-1}]

$Q_{t,i} = Q_{r,i} + Q_{b,i}$= streamflow at timestep i [L^3T^{-1}]

α= recession constant (ranging between 0 and 1) [-]

BFI_{max}= long-term ratio of baseflow to total streamflow (ranging between 0 and 1) [-]

From the streamflow hydrograph, recession periods were identified and extracted to calculate the recession constant. Relatively short recession periods (< 10 days) were excluded to minimize noise from other hydrological processes or anthropogenic effects, such as abstractions. Based on median values across the studied subcatchments, a representative α value of 0.95 was adopted. The parameter sensitivity was evaluated by varying α from 0.93 to 0.97. As streamflow at the catchment outlet is perennial, a relatively high long-term contribution of baseflow to total streamflow (BFI_{max}) is expected. Accordingly, the Eckhardt separation method was applied using $BFI_{max} = 0.8$. Sensitivity analyses were also performed using lower BFI_{max} values of 0.6 and 0.7. The resulting baseflow values were also compared with those obtained using the aforementioned graphical methods as presented in Table S2.

3.3. Water balance

A water balance was developed for the Wundanyi catchment for the years 2023, 2024 and 2025, and for the four other studied subcatchments (Ruma, Iyale, Ngangao and Dembwa) for the year 2024. Results were also aggregated for the Wundanyi mountain subcatchments (Ruma, Iyale and Ngangao), hereafter referred to as "Upper Wundanyi (UW)", and for the remaining lower Wundanyi subcatchments, hereafter referred to as "Lower Wundanyi (LW)". At Ruma, discharge was estimated from continuous water-level records obtained from the pressure transducer installed at the subcatchment's outlet. For Iyale and Ngangao, discharge was estimated as the difference between the records from the nested Ruma, Wundanyi and Mwangoto monitoring locations. The contribution of the Upper Wundanyi (UW) to the total streamflow of the Wundanyi catchment (W) was evaluated for 2024 as:

$$C_{UW} = \frac{Q_{t,UW}}{Q_{t,W}} \quad (2)$$

Where:

C_{UW}= Upper Wundanyi contribution [-]

$Q_{t,UW}$= total streamflow of the Upper Wundanyi subcatchment [L^3T^{-1}]

$Q_{t,W}$= total streamflow of the Wundanyi catchment [L^3T^{-1}]

Since streamflow was derived from continuously measured water levels, the resulting values represent the streamflow remaining after abstractions. Field surveys identified relatively few wells within the Wundanyi catchment, suggesting that groundwater abstractions may have had a limited effect on baseflow.

For the water balance calculations, rainfall and temperature were assigned using data from existing stations and adjusted to the median catchment elevation using elevation gradients derived from available station data. Actual evapotranspiration (ET_a) was calculated using the Turc empirical method (Turc, 1955). Assuming negligible change in storage ($\Delta S \approx 0$), lateral subsurface flow (Q_{ls}) was estimated as the residual of the water balance, and calculated as the difference between precipitation (P), measured streamflow (Q_t), calculated ET_a, and abstractions (Q_d) for domestic and agricultural water uses. Population data were obtained from the 2019 Kenya Population and Housing Census (Kenya National Bureau of Statistics, 2019). Domestic water use was assumed to range between 17 L capita^{-1} day^{-1} in the lowlands, corresponding to the recommended value for arid and semi-arid rural areas in Kenya (Afullo et al., 2014), and 38 L capita^{-1} day^{-1} in the highlands, consistent with reported values for rural areas in Kenya (Wagner et al., 2019). Livestock data were derived from Kenya National Bureau of Statistics (2015), and a livestock unit (LU) water consumption rate of 50 L LU^{-1} day^{-1} was adopted from the Kenyan Ministry of Water and Irrigation (2005). Irrigation was assumed to occur within a 250 m buffer on each side of high-order streams, at an application rate of 5000 m^3 ha^{-1} yr^{-1}, and only within agroforestry and croplands. Q_d was estimated for the Wundanyi catchment and converted to an equivalent areal demand rate. Due to the lack of more local data, this rate was applied uniformly to all subcatchments, while the volumetric demand was calculated by multiplying the rate by the subcatchment area. Since direct measurements of water withdrawals were not possible across the catchment, water demand was assumed to be equivalent to actual withdrawals.

Under natural conditions, recharge represents the rainfall remaining after actual evapotranspiration and stormflow ($P\text{-}ET_a\text{-}Q_r$). The values of P and ET_a were the same as those used in the water balance calculations described above, while Q_r was obtained using the adopted baseflow separation method and parameters (Section 3.2).

The TerraClimate dataset (Abatzoglou et al., 2018) was used for validation purposes, mainly for actual evapotranspiration and total runoff.

3.4. Chloride mass balance for recharge estimation

Groundwater recharge was calculated using the chloride mass balance, initially developed by Eriksson and Khunakasem (1969), which requires the collection and analysis of rainwater and groundwater samples. A total of 51 rainwater samples were collected from six locations (Fig. 2) between February 2024 and October 2025. Rainwater samples with chloride concentrations exceeding 10 mg/L were discarded to remove the influence of extreme, unrealistic values. Rainfall depth was then incorporated by calculating rainfall-weighted average chloride concentrations, in which each rainwater sample was weighted by the rainfall amount of its sampling period. The elevation-dependent rainfall and chloride gradients were respectively used to assign representative rainfall and rainwater chloride concentrations to individual locations (the springs in Fig. 2) where the chloride mass balance (CMB) method was applied. Hydrochemical and isotopic evidence presented by Khan (2022) indicated that most springs considered in this analysis are locally recharged, which justifies using rainfall and chloride values corresponding to the spring elevation. However, for springs with larger springsheds (namely Mwangoto, Embelonyi, and Mbumbunyi), spatially averaged rainfall and chloride values were adopted.

The CMB method integrates the root zone water balance and the transport of chloride through this zone. Chloride introduced via precipitation and dry atmospheric deposition may infiltrate the root zone and subsequently percolate toward the groundwater table. Since chlo-

ride precipitation within the root zone is unlikely, and assuming that no additional natural or anthropogenic sources of chloride are present, the chloride mass balance can be expressed as (Nonner, 2002):

$$P.Cl_P + D_d = Q_{prec}.Cl_{Q_{prec}} + Q_r.Cl_{Q_r} + S_{root}.Cl_{S_{root}} \quad (3)$$

Where:

P= precipitation rate [LT^{-1}]

Q_{prec}= rate of percolation at the lower boundary of the root zone (i.e., actual groundwater recharge) [LT^{-1}]

Q_r= stormflow [LT^{-1}]

S_{root}= water stored or released in the root zone (i.e., soil water) [LT^{-1}]

D_d= dry deposition flux of chloride [$ML^{-2}T^{-1}$]

Cl_P, Cl_{Q_r}, $Cl_{Q_{prec}}$ and $Cl_{S_{root}}$= chloride concentration in precipitation, stormflow, percolating groundwater (recharge water), and soil water, respectively [ML^{-3}]. Q_r values were identified for each subcatchment using hydrograph separation techniques (see Section 3.2), and the corresponding value was assigned to each calculation point according to its subcatchment.

Alcalá and Custodio (2008) and Appelo and Postma (2004) reported that when rain collectors are permanently exposed, dry-deposited chloride is likely to be already incorporated into the bulk rainwater samples. As the collectors in the present study were permanently exposed, the dry deposition term (D_d) was tentatively assumed to be included in $P.Cl_P$. Assuming steady-state conditions with no changes in root zone salinity, and assuming that the chloride concentration in stormflow is similar to that of precipitation due to rapid runoff generation in the study area, the chloride mass balance can be rewritten as:

$$Q_{prec} = (P - Q_r).\frac{Cl_P}{Cl_{Q_{prec}}} \quad (4)$$

The recharge ratio can then be expressed as a fraction of rainfall after estimating the runoff coefficient ($C_r = Q_r/P$):

$$\frac{Q_{prec}}{P} = (1 - C_r).\frac{Cl_P}{Cl_{Q_{prec}}} \quad (5)$$

CMB-derived recharge values were averaged at the (sub)catchment scale using discharge-weighted averages, after excluding springs potentially affected by additional, non-atmospheric chloride inputs. Weights were assigned according to spring discharge class: 10 for very high-discharge (> 30 L/min) springs, 5 for high-discharge (10-30 L/min) springs, and 1 for medium- and low-discharge (< 10 L/min) springs. These weights were selected to prevent small springs from exerting a disproportionate influence on the subcatchment-scale average recharge values. Sensitivity analyses were performed using alternative 3-2-1 and 5-3-1 weighting schemes.

A multivariable linear regression analysis, including the 60 distinct springs shown in Fig. 2 and Fig. 6, was conducted to estimate the effects of dominant lithology, vegetation type, elevation, slope steepness, and structural geology on groundwater recharge. Since lithology and vegetation type are qualitative variables, they were represented using dummy variables, with banded biotite gneiss and agroforestry used as the respective reference classes. Distance to the nearest lineament was used as a proxy for structural geology and was log-transformed because of its skewed distribution. The relative importance of each factor was then evaluated using the partial coefficient of determination (partial R^2), and significance was assessed using partial F-tests. Classes represented by fewer than three observations were excluded from the multivariable regression analysis. A second multivariable linear regression analysis was performed with all five predictors represented as dummy variables, and classes represented by fewer than three observations were merged into relatively similar groups.

3.5. Water chemistry

Field campaigns included in situ water quality measurements and sampling for major ions and tritium analyses. Electrical conductivity (EC), pH, and water temperature were measured using portable Hanna multiparameter probes (HI98194, HI98195, HI98196). Alkalinity and silica were also measured in the field using portable Hanna Checkers (HI775 and HI770, respectively). Two targeted campaigns were carried out between mid-February and early March 2024 (dry season) and between mid-April and mid-May 2024 (wet season), during which 46 and 51 water features were sampled, respectively (Fig. 2). Three rain collectors were installed at Ngangao (highland), Irido (transition zone), and Msau (lowland) during the mission of February-March 2024 to collect rainwater samples for chloride analysis. The October 2024 mission, conducted toward the end of the dry season (i.e., before the onset of the short rains), focused on collecting six spring, seven stream, and six rainwater samples for tritium analysis. An additional mission was conducted in February 2025 to fill remaining sampling gaps, mainly shallow and deep groundwater samples from existing wells. During this mission, three new rain collectors were also installed in Wesu (highland), Wundanyi (transition zone), and Mbale (lowland), to address spatial gaps and to validate data from existing rain collectors.

For major ion analysis, two 20 mL samples were collected per site in polyethylene bottles and filtered through 0.45 µm cellulose filters. As recommended by Appelo and Postma (2004), two to three drops of 65% nitric acid (HNO_3) were added to the samples designated for cation analysis to prevent oxidation, limit cation adsorption or precipitation, and prevent bacterial growth. The samples were stored at a cool temperature to reduce microbial activity and maintain chemical stability. Concentrations of major cations, iron, and manganese were measured at IHE Delft's laboratory using Inductively Coupled Plasma Optical Emission Spectrometry (ICP-OES). Ion Chromatography (IC) was used to determine chloride, sulfate, nitrate, and fluoride concentrations. Tritium samples were collected in 1 L polyethylene bottles and analyzed at the laboratories of Hydroisotop GmbH (Germany). Tritium activity was measured by liquid scintillation counting (LSC) following electrolytic enrichment (detection limit: 0.6 TU). Results are reported in tritium units (TU) with double standard deviation.

Measured tritium activities from 2024 were projected backward in time, assuming radioactive decay only, using the exponential decay equation with a tritium half-life ($T_{1/2}$) of 12.32 years (Clark and Fritz, 2013):

$$C(t) = C_0 \exp(-\lambda t); \lambda = \frac{\ln(2)}{T_{1/2}} \quad (6)$$

Where:

$C(t)$: tritium activity (expressed in TU) at time t

C_0: initial tritium activity at recharge (expressed in TU)

λ : decay constant [T^{-1}]

t : elapsed time since recharge [T]

$T_{1/2}$: tritium half-life [T]

Lindsey et al. (2019) reported that tritium levels had clearly stabilized by 2008-2012 in the United States. In the absence of local studies on this matter, modern rainfall measured in the Taita Hills in 2024, with an average tritium activity of 1.6 ± 0.5 TU, was assumed to be representative of precipitation tritium levels from 2010 to 2024. The intersection between a spring's backward decay curve and the precipitation tritium range provides an indicative recharge time for the sampled water. This method is not novel in principle as it simply assumes radioactive decay under piston-flow conditions. However, the way it is implemented here constitutes a simplified, study-specific adaptation in the absence of local historical tritium records. For highland springs, the intersection was determined using the decay curve of highland rainwater, whereas for the transition zone and lowland springs, the average (highland and lowland) tritium activity was used. As this approach

assumes piston flow conditions, it does not account for mixing or dispersion processes.

The desktop hydrochemical analysis comprised classification of chemical water types following Stuyfzand (1989) and the use of various scatter plots.

4. Results

This section presents key findings, progressing from rainfall patterns and water balance analyses to streamflow dynamics, groundwater recharge calculations, water chemistry, and groundwater residence times.

4.1. Rainfall analysis

Linear regression indicates a stronger rainfall-elevation gradient of +89 mm per 100 m increase in elevation on the eastern and southeastern windward side, compared to +35 mm per 100 m on the leeward side (Fig. 3a). The monthly rainfall distribution at the windward stations shows a clear bimodal pattern, with peaks during the long rains in April and the short rains in November (Fig. S4). Rainwater chloride concentrations between February 2024 and October 2025 (Fig. S5) range from 0.1 mg/L (recorded at Ngangao) to 7.8 mg/L (recorded at Irido), with a few exceptional anomalies exceeding 10 mg/L. The lowest concentrations occur during the rainy seasons when more frequent and larger rainfall events dilute atmospheric dust, whereas chloride content generally increases during the dry season. Based on rainfall-weighted averaging (see Section 3.4), a rainwater chloride gradient with respect to elevation is generally observed, with higher chloride concentrations (around 1.4 mg/L) in the lowlands than in the highlands (around 0.9 mg/L), as shown in Fig. 3b.

4.2. Stormflow vs. baseflow

Fig. 4 shows the time series of calculated stream discharge at the eight selected monitoring sites in the Wundanyi and Mwatate catchments. Average discharge of the entire Wundanyi catchment (measured at Msau station) is around 274 L/s (174 mm/y). Compared to rainfall (P) in 2024 (even though discharge does not correspond to 2024 rainfall only), total discharge (Q_t) accounts for 16.5% of P, much lower than in its three mountainous subcatchments, Ngangao, Ruma, and Iyale, where Q_t accounts for 29.2% of P (Table 1). Moreover, Q_t of the mountainous subcatchments of Wundanyi (i.e., Upper Wundanyi) is approximately seven times higher than Q_t of Lower Wundanyi in 2024. If we add river abstractions (Q_d) to the total flow, Q_t+Q_d accounts for 23.0% of P for the total catchment and 34.9% of P for Upper Wundanyi.

Stream discharge largely follows rainfall patterns, with peaks occurring due to stormflow shortly after the heaviest rainfall. During certain storm events, the continuously monitored stages exceeded the maximum gauged stage (Table S1). Varying the extrapolated discharge estimates by ±30% changes the total annual discharge by ±2.6 to 4.1% at Wundanyi, ±3.2 to 10.1% at Msau, ±1.9 to 3.0% at Mwangoto, and ±14.7 to 15.9% at Ruma. For records shorter than one year, the effect on total discharge ranges from ±5.5% to ±12.0%. Hydrograph separation results, namely Q_r, Q_b, and the derived variables, for the studied subcatchments for the year 2024 (the year for which all have data) are included in Table 1. Stormflow (Q_r) exhibits flashy peaks and totals 4.3% of total rainfall (P) and 26.4% of total discharge (Q_t) within the Wundanyi catchment, or 18.9% if river abstractions (Q_d), affecting mostly river baseflow (Q_b), are included in the total flow.

The median recession constant for the Wundanyi catchment is 0.94 and is quite consistent across subcatchments, ranging from 0.94 to 0.96. The adopted parameterization discussed in Section 3.2 results in a BFI of 74% for the Wundanyi catchment, consistent with the 74-80% range obtained using the graphical separation methods of Pettyjohn and Henning (1979) (Table S2). Based on the adopted parameterization, baseflow corresponds to approximately 12% of total rainfall between 2023 and 2025. The resulting baseflow hydrograph is shown in Fig. S6. BFI values are relatively consistent, with the highest values 0.77 and 0.79 in the subcatchments of Iyale and Dembwa (see location in Fig. 2), respectively. The baseflow proportion of rainfall is much more variable, ranging from a minimum of 9% in Dembwa to a maximum of 33% in Iyale. This variability is most likely related to lateral subsurface flows, which affect the observed baseflow values at the subcatchment level.

4.3. Spring vs stream discharge

Many highland springs have similar discharge at the end of the dry season (February 2024) and a month after the start of the wet season (April 2024), clustering close to the 1:1 line, although the higher discharge springs tend to show a lower discharge in April than in February (Fig. 5). The latter is seen more strongly for springs emerging in the transition zone, with one exception. For these springs, the median April-to-February discharge ratio is 0.19, with an interquartile range (IQR) of 0.16-0.21 (n = 5). These springs, therefore, show a continued recession despite the start of the rains.

Stream discharge is clearly more significant in April. Overall, the median April-to-February discharge ratio is 2.33, with an IQR of 2.09-

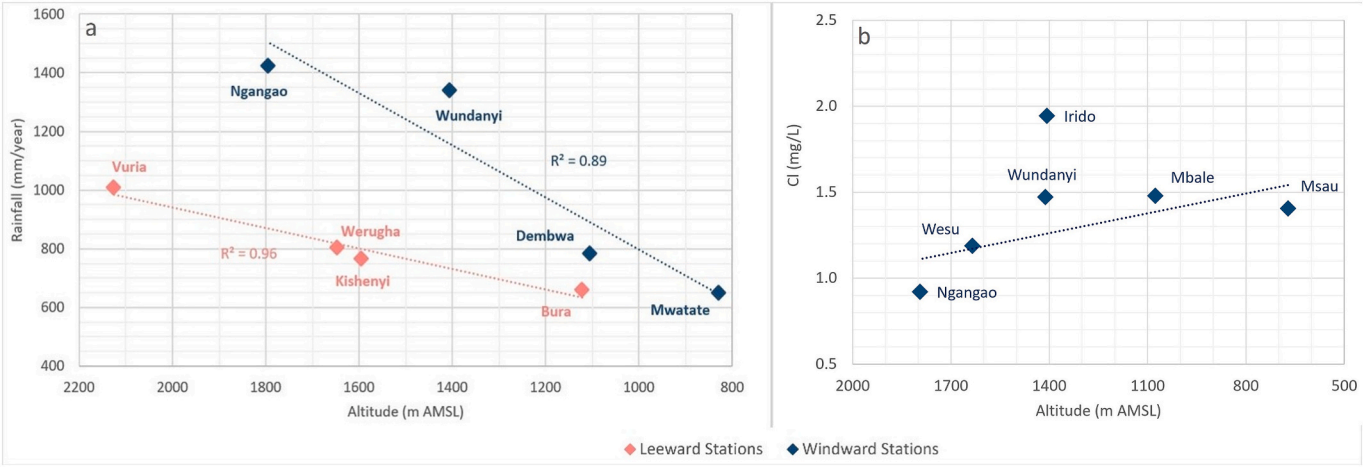


Fig. 3. Relationships between altitude and (a) arithmetic mean annual rainfall (2012-2024, based on data availability) and (b) rainfall-weighted mean chloride concentrations (February 2024-October 2025). The trend line in panel (b) excludes Irido, which may be influenced by local atmospheric circulation or deposition effects.

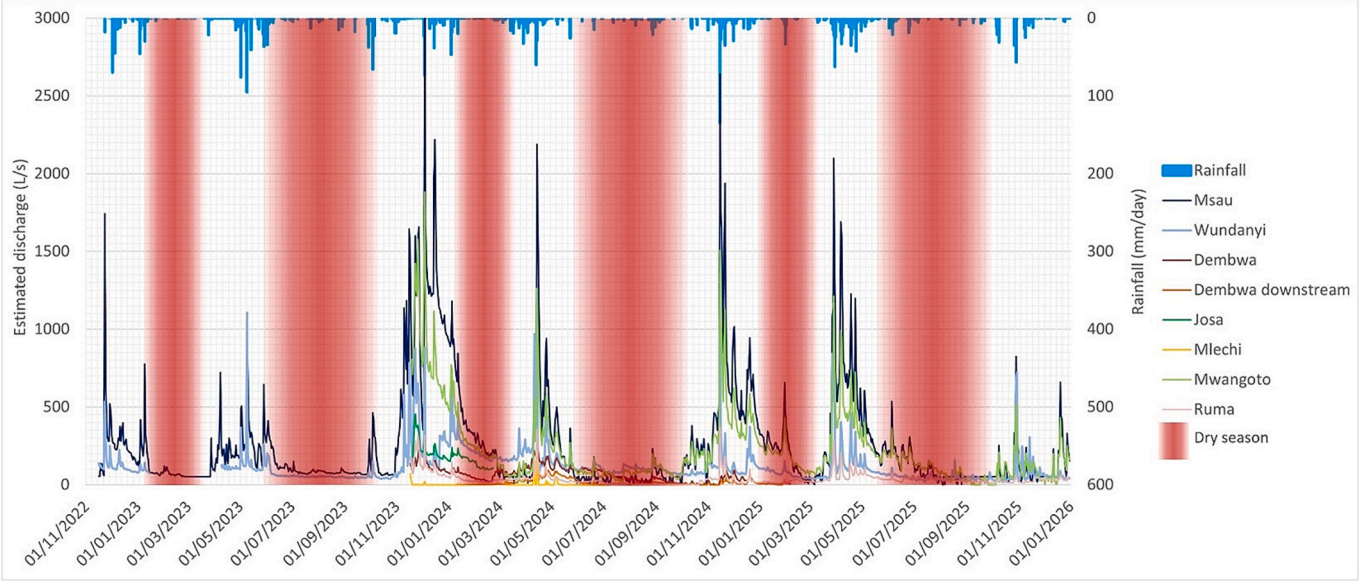


Fig. 4. Time series of calculated total stream discharge (total streamflow) at selected monitoring sites in the Wundanyi and Mwatate catchments, together with Wundanyi daily rainfall. Shaded red bands indicate typical dry-season periods. The y-axis is truncated at 3000 L/s to improve visualization of low-flow values; the peak value in December 2023 reached 3520 L/s. Daily rainfall data source: Taita Research Station/University of Helsinki.

Table 1
Characteristics and derived hydrological indicators for the year 2024 for the studied subcatchments.

Variable (units)	Description	Ngangao (UW1)	Ruma (UW2)	Iyale (UW3)	Upper Wundanyi (UW = UW1+UW2+UW3)	Lower Wundanyi (LW)	Wundanyi (W=UW+LW)	Dembwa
A (km^2)	(Sub)catchment area	10.0	3.8	7.7	21.5	28.0	49.5	18.5
Z_{med} (m AMSL)	Median elevation	1575	1570	1570	1572	1285	1410	1260
Main Lithology (% A)	Soil overlying Precambrian basement	52	87	85	70	17	40	49
	Gneiss	45	13	15	28	75	55	51
Vegetation type (% A)	Montane forest	13	3	2	8	3	5	3
	Plantation forest	10	11	15	12	3	7	2
	Agroforestry	57	76	74	67	21	41	41
	Thicket	7	0	0	3	66	39	41
	Cropland	12	10	8	10	5	7	12
f (cm/h)	Average infiltration rate	78	63	63	70	54	60	59
P (mm/y)	Total annual rainfall	1204	1199	1199	1201	946	1057	924
ET_a (mm/y)	Actual evapotranspiration	819	817	817	818	781	810	745
Q_t (m^3/d)	Total streamflow	7288	2435	10935	20658	2982	23640	5420
Q_t (mm/y)	Total streamflow	267	231	518	350	51	174	107
Q_r (mm/y)	Stormflow	71	62	120	87	14	46	23
Q_b (mm/y)	Baseflow	196	169	398	264	37	128	84
Q_d (mm/y)	River abstractions	69	69	69	69	69	69	69
C_r (%)	Runoff coefficient	5.9	5.2	10.0	7.2	1.5	4.3	2.5
BFI (% Q_t)	Baseflow index	73.5	73.0	76.9	75.2	72.4	73.6	78.6
Q_b/P (%)	Baseflow proportion of total rainfall	16.3	14.1	33.2	21.9	3.9	12.1	9.1
$Q_{prec,\ natural}$ (mm/y)	Groundwater recharge (natural conditions)	314	320	262	297	151	201	155
Q_{ls} (mm/y)	Lateral subsurface outflow	49	82	-205	-36	46	4	3

Note: lithology and vegetation type classes may not sum to 100% due to minor classes not included in this table. Average infiltration rates are calculated based on Table S5. Median subcatchment slope varies from 25% in Iyale to 30% in Ngangao.

3.30 (n = 17). As also shown in Fig. 5, stream discharge is much greater than the combined discharge of all springs during both the dry season (by a factor of 5) and wet season (by a factor of 10), noting that the observed difference cannot be explained by unmapped springs. As no large springs were excluded from this analysis, these results likely indicate substantial subsurface contributions to streamflow along faults and fracture zones.

4.4. Specific discharge

The spatial distribution of specific discharge across the Wundanyi and Mwatate subcatchments for February 2025, representing dry-season conditions and therefore baseflow, is presented in Fig. 6. The south-western subcatchments of the Wundanyi catchment, including Ruma and Iyale subcatchments, have the highest specific discharge, ranging from 0.29 to 0.38 L/d/m^2, with a median of 0.33 and an IQR of 0.30 to 0.36 (n = 5). Together covering around 11% of the study area, these high specific discharge subcatchments also show the highest spring density with 1.6 springs/km^2, which is double the average spring density across the entire study area (0.8 springs/km^2). Moreover, the four subcatchments include approximately one third of the high- and very high-discharge springs. It is also worth noting that the lineament

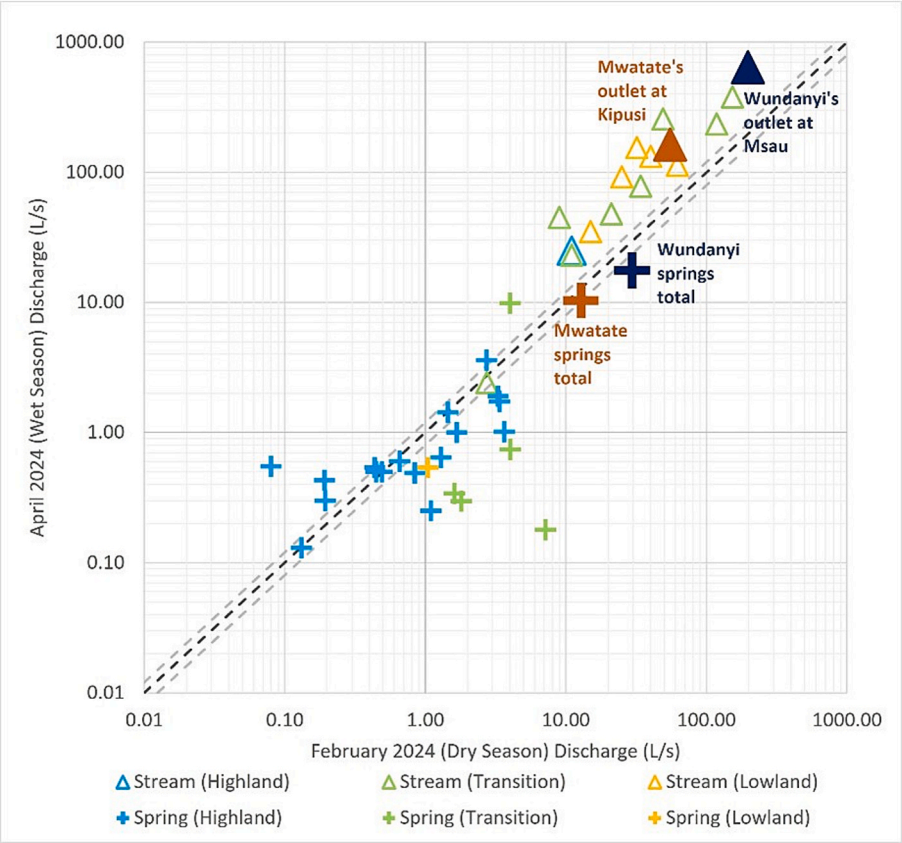


Fig. 5. Comparison of stream and spring discharge measured in February 2024 (dry season) and April 2024 (wet season) across the Wundanyi and Mwatate catchments. Outlet and aggregated spring discharges are indicated for each catchment. The black dashed line represents the 1:1 relationship, while the grey dashed lines indicate a ±20% relative deviation from the 1:1 line.

orientation in the study area is predominantly north-south, with many springs emerging near these structures.

4.5. Rainfall partitioning and catchment water balance

Table 1 summarizes the main characteristics of the studied subcatchments and the derived hydrological variables from baseflow separation and water balance analyses for 2024. Results of Table 1 are expressed as a fraction of rainfall in Table S3. Spatially averaged annual rainfall ranges from 924 mm in Dembwa to about 1200 mm in the Upper Wundanyi subcatchments. Most rainfall is lost through evapotranspiration, accounting for approximately 68% in the Upper Wundanyi subcatchments and 81-83% in Dembwa and the Lower Wundanyi subcatchments. Under natural conditions, groundwater recharge derived from rainfall partitioning ranges from about 150 mm/y (16.0% of rainfall) in the Lower Wundanyi to 320 mm/y (26.6% of rainfall) in Ruma, one of the Upper Wundanyi subcatchments. Taken together, the Upper Wundanyi subcatchments show a recharge value of about 300 mm/y (24.7% of rainfall). At the Wundanyi catchment scale, a recharge value of approximately 200 mm/y (19.0% of rainfall) is obtained.

In 2024, the total streamflow from the Upper Wundanyi subcatchments (Ruma, Iyale, Ngangao) is 20658 m^3/d, compared with 23640 m^3/d at the Wundanyi catchment outlet at Msau. As a result, the Upper Wundanyi subcatchments, covering 43% of the Wundanyi catchment area, contribute to 87% of its total discharge in 2024, pointing towards a disproportionate contribution from the highlands. When including abstractions in the total flows (i.e. simulating a natural system) this percentage decreases to 75%. Iyale has the highest baseflow contribution (33% of rainfall) and runoff coefficient (10%), both of which are two to four times higher than those of the other studied subcatchments. The results also indicate lateral subsurface outflows of 82 and 49 mm/y from the northern Ruma and Ngangao subcatchments, respectively. In contrast, the southernmost Iyale subcatchment, which forms the remainder of the Upper Wundanyi subcatchment, receives a lateral subsurface inflow of 205 mm/y, most likely originating from Ruma and Ngangao. At the Wundanyi catchment scale, as well as at the Dembwa subcatchment scale, the water balance largely closes, indicating negligible lateral subsurface flow in 2024. At the Wundanyi catchment scale, baseflow and abstractions together amount to 197 mm/y, a value that closely matches the estimated natural groundwater recharge of 201 mm/y (19.0% of rainfall). The same is observed for the Dembwa subcatchment, but with lower baseflow and recharge values.

Results for the Wundanyi catchment for the years 2023-2025 are presented in Table S4, noting that ET_a accounted for approximately 75% of total rainfall in 2023 and 84% in 2025, while total discharge represented 17.2% and 14.9% of annual rainfall in 2023 and 2025, respectively. When river abstractions are also considered, and assuming limited net lateral subsurface flow from the catchment, the change in storage varies from 2.0% of rainfall in 2023 to 0.4% in 2024 and -8.3% in 2025. Overall, the storage decreased from 2023 to 2025, consistent with a decline in rainfall from 1077 mm in 2023 to 787 mm in 2025, along with increases in actual evapotranspiration and abstractions.

The TerraClimate dataset indicates average actual evapotranspiration and total discharge of 79% and 17% of total rainfall, respectively, for the Wundanyi catchment over the period 1958-2024, consistent with the values obtained in our analysis.

4.6. Groundwater recharge

The groundwater recharge analysis using the chloride mass balance

method indicates average recharge ratios of 10.9 ± 4.7% of rainfall in February 2024 (dry season) and 11.3 ± 4.8% in April 2024 (wet season). Sungululu and Mangalasenyi springs are excluded from the comparison due to anthropogenic contamination at Sungululu, and consistently high recharge ratios at Mangalasenyi (> 35% of rainfall, on average) that likely reflect localized recharge conditions. Most springs cluster closely around the 1:1 line of wet vs dry season values (Fig. 7), with deviations of less than ±2.5%, suggesting that these ratios reflect long-term recharge conditions rather than short-term seasonal variability. The Wilcoxon signed-rank test shows that the test statistic ($W = 101$) exceeds the critical value ($W_{critical} = 65$) at a 95% confidence level ($n = 22$). The null hypothesis of "no difference between February and April recharge ratios" can therefore not be rejected, indicating that the two sets of values are not statistically different.

Including the springs sampled by Khan (2022) to this analysis, actual recharge, expressed in mm/y, tends to be higher in the highlands (155 ± 66 mm/y) than in the transition zone (124 ± 52 mm/y). The highest recharge ratios, expressed as proportion of total rainfall, are obtained in areas covered by plantation forests ($n = 12$) and agroforestry ($n = 37$), with respective values of 12.8 ± 4.4% and 10.5 ± 4.1% of rainfall. Springs classified in the montane forests class ($n = 7$) have a markedly low calculated recharge of 6.7 ± 2.0% of rainfall (Table S6). Obtained recharge values are overall much lower than those obtained through the rainfall partitioning method (Section 4.5). The multivariable regression model explains about 21% of the variability in groundwater recharge ($R^2 = 0.21$), although the overall model is not statistically significant at the 95% confidence level ($p = 0.12$). Vegetation type shows the largest independent contribution to recharge variability (partial $R^2 = 0.16$) and is the only statistically significant factor based on the partial F-test ($p = 0.02$). However, the significance of the partial F-test for vegetation type should be interpreted cautiously since the overall model is not statistically significant. Relative to agroforestry, the modeled recharge ratio is 3.0% of rainfall lower under montane forest and 3.2% of rainfall higher under plantation forest. Lithology shows the second-largest independent contribution (partial $R^2 = 0.03$), while the remaining factors have partial R^2 values of approximately 0.01 or lower. The second multivariable regression model, in which all five predictors are represented as dummy variables, gives similar overall conclusions, with vegetation remaining the only statistically significant factor.

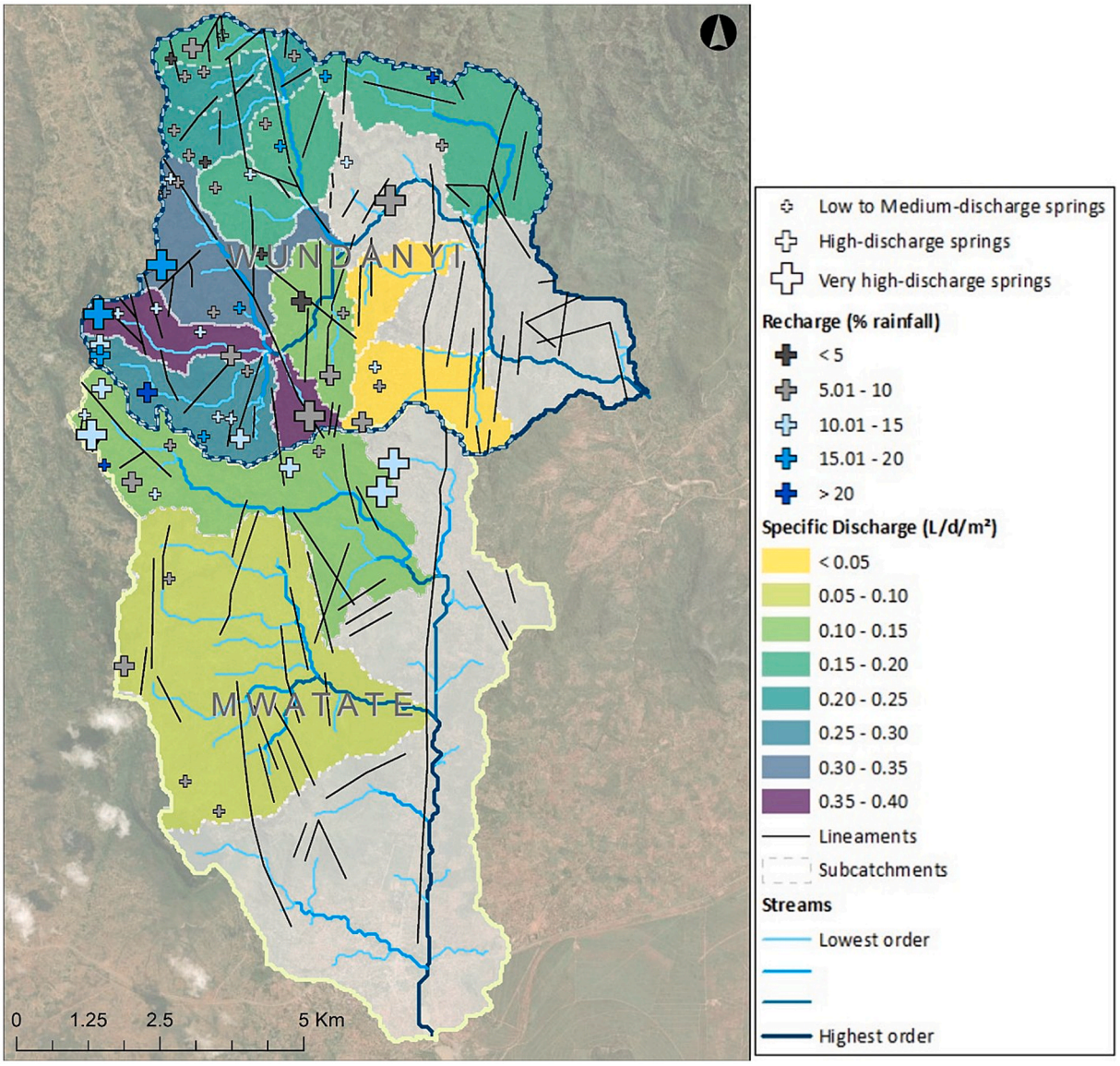


Fig. 6. Spatial distribution of springs sampled by the authors in 2024 and by Khan (2022), including spring discharge classes and CMB-derived recharge ratios, together with specific discharge across the Wundanyi and Mwatate subcatchments.

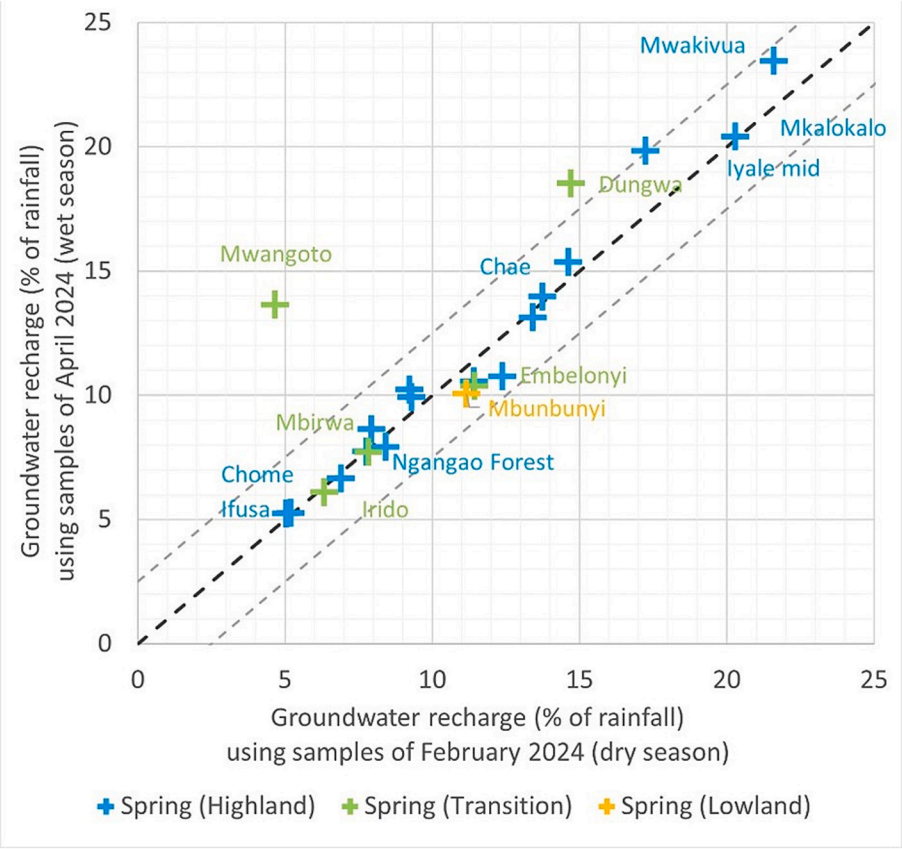


Fig. 7. Groundwater recharge values derived using the CMB for springs in February 2024 (dry season) and April 2024 (wet season). The black dashed line represents the 1:1 relationship, and the grey dashed lines indicate a ±2.5% offset from this line.

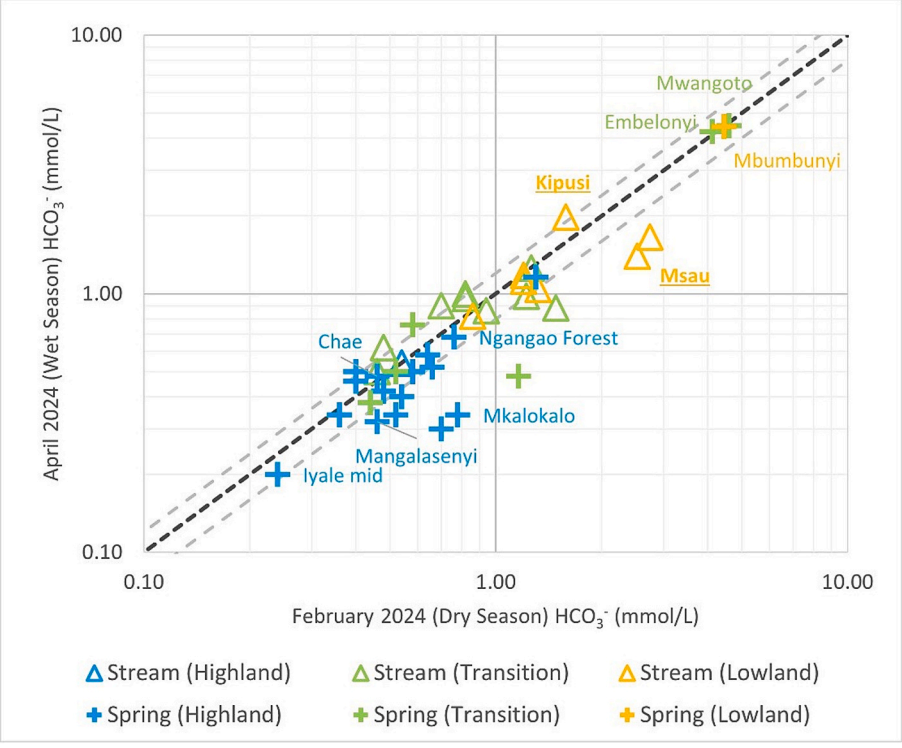


Fig. 8. Comparison of bicarbonate concentrations measured in February 2024 (dry season) and April 2024 (wet season) for springs and streams across the Wundanyi and Mwatate catchments. The black dashed line represents the 1:1 relationship, while the grey dashed lines indicate a ±20% relative deviation from the 1:1 line.

4.7. Hydrochemical analysis

Lowland samples generally have the highest bicarbonate and EC values (Fig. 8 and Fig. 9). For instance, HCO_3^- concentrations in February 2024 are approximately 4.5 mmol/L for the Mbumbunyi spring and 1.63 ± 0.72 mmol/L for the seven lowland stream samples. For stream samples, EC increases linearly with decreasing altitude (i.e., along the flow direction), with a regression slope of 23 µS/cm per 100 m decrease in elevation and a coefficient of determination (R^2) of 0.76. The grouped results (Table S7) show an increase in mineralization toward lower elevations; median EC and HCO_3^- increase from 100 µS/cm and 0.64 mmol/L in the highlands to 278 µS/cm and 2.52 mmol/L in the lowlands, respectively. Deep wells have the highest median EC, HCO_3^-, and dissolved Si values, with the most mineralized deep wells situated in the lowlands. However, even when deep wells are excluded, the downgradient increase in mineralization remains evident in springs and streams.

Bicarbonate (HCO_3^-), often reflecting water-rock interaction, shows strong seasonal stability in the regularly monitored springs and streams (Fig. 8). The median April-to-February (i.e., wet-to-dry) alkalinity ratio is 0.92, with an IQR of 0.79-1.03 (n = 41). However, some springs and streams deviate from the 1:1 line, notably the Msau stream, which shows a decrease in HCO_3^- concentration from approximately 2.5 mmol/L in the dry season to about 1.4 mmol/L in the wet season, indicating a greater contribution of older groundwater during the dry season.

Fig. 9 shows that $CaHCO_3$ water types dominate across most of the elevation range (between 620 and 1660 m AMSL), while $NaHCO_3$ water types occur more locally, mainly at higher elevations (i.e., above 1660 m AMSL). The figure also shows increasing EC values with decreasing elevation, indicating progressive mineralization. Spring EC values show a non-linear relationship with altitude, whereas stream EC values show a more linear downstream increase, consistent with cumulative baseflow contributions.

Most lowland and transition zone samples, as well as many highland samples, fall within the rock-dominance field of the Gibbs diagram, indicating that water-rock interaction is the main control on hydrochemistry, with only a minor influence from evaporation (Fig. S7). Ca^{2+}/Na^+ ratios between 0.2 and 2 coupled with Mg^{2+}/Na^+ ratios between 0.1 and 1.0 (Fig. S8) as well as the coupled increase in bicarbonate and dissolved silica (Fig. S9), further confirm that silicate weathering, involving the dissolution of feldspar minerals such as albite ($Na(AlSi_3)O_8$), as well as amphibole (glaucophane: $Na_2(Mg_3Al_2)Si_8O_{22}(OH)_2$), or biotite ($K(Mg_2Fe)(AlSi_3)O_{10}(OH)_2$), is the dominant geochemical process.

Highland samples have an average HCO_3^-/Si ratio of 2.00 ± 0.85, whereas transition zone and lowland samples have respective average ratios of 4.38 ± 2.70 and 5.61 ± 0.85, possibly indicating changes in the dominant silicate weathering reactions or localized carbonate dissolution associated with marble units.

In the lowlands of the Mwatate catchment, deep groundwater shows relatively elevated salinity, with EC values exceeding 2000 µS/cm in one deep well (reported borehole depth of approximately 200 m). In contrast, the deep wells visited in the highlands have EC values below 500 µS/cm, indicative of fresh groundwater (Fig. S10). This observation suggests longer groundwater residence times, lower recharge and more extensive water-rock interaction in the lowlands, as well as pointing towards limited regional subsurface freshwater flow (i.e. longer flow paths) from the highlands, as suggested by the water balance analysis.

On another note, measured fluoride concentrations range from <0.1 to 0.66 mg/L (detection limit = 0.1 mg/L), well below the WHO guideline value of 1.5 mg/L for drinking water (WHO, 2017).

4.8. Tritium patterns and relative residence times

Rainwater samples show average tritium levels of 1.6 ± 0.5 TU, with generally higher values at higher elevations. In the highlands (Ngangao), rainwater tritium values of 1.6 and 1.9 TU yield an average of 1.75 TU, while in the transition zone (Irido), values of 1.6 and 2.4 TU correspond to an average of 2.0 TU. In contrast, lowland rainwater samples collected at Msau show lower tritium levels of 1.1 and 1.2 TU, with an average of 1.15 TU (Fig. 10 and Fig. S11). The closest long-term monitoring station in the IAEA's Global Network of Isotopes in Precipitation (GNIP) database is Dar es Salaam, Tanzania. Available post-peak tritium activity values from Dar es Salaam are shown in Fig. 11. Based on

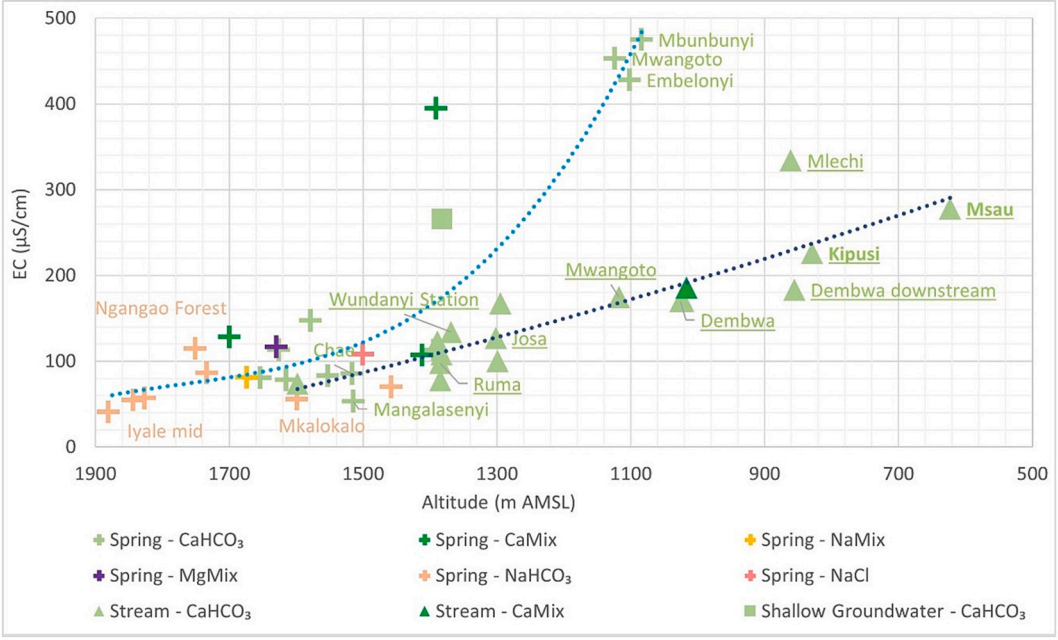


Fig. 9. Relationship between electrical conductivity (EC) measured in February 2024 and altitude. Samples are classified by water source type and chemical type. The dashed light blue line represents a third-order polynomial fit ($R^2 = 0.82$) to all spring samples, while the dashed dark blue line represents a linear fit ($R^2 = 0.76$) to all stream samples.

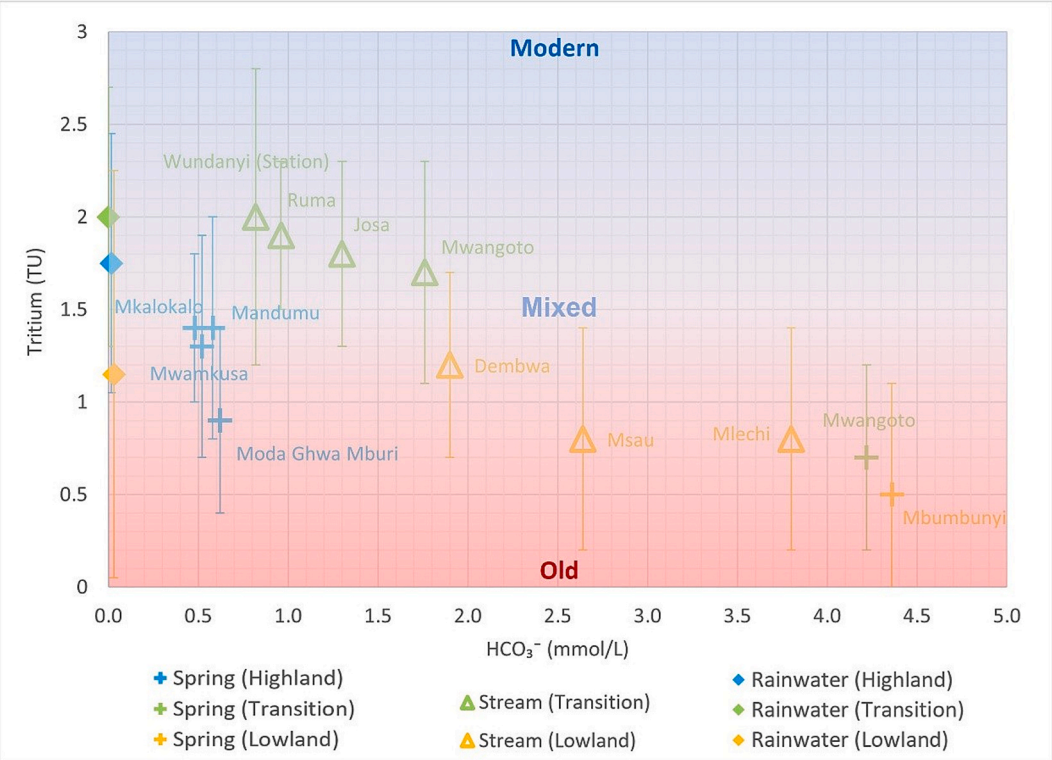


Fig. 10. Relationship between tritium activity (TU) and bicarbonate concentration (HCO_3^-) in springs and streams across the Wundanyi and Mwatate catchments. Rainwater tritium activity values are shown at $HCO_3^- \approx 0$ mmol/L for reference, as alkalinity was not measured and is expected to be negligible in precipitation. Error bars represent the analytical uncertainty of tritium measurements as reported by the laboratory. Shaded fields indicate conceptual groundwater age domains for coastal and low-latitude regions based on the qualitative interpretation of Clark and Fritz (2013).

radioactive decay, the 1964 bomb-peak tritium activity of approximately 48 TU at this station would have decayed to about 1.6 TU by 2024, a value similar to tritium levels measured in present-day, modern rainwater in the Taita Hills. This similarity may complicate the distinction between recharge from the early to mid-1960s and recent recharge.

Stream samples have average tritium levels of 1.5 ± 0.5 TU; streams in the transition zone show a modern tritium signature, with an average value of 1.9 ± 0.1 TU, whereas lowland streams have tritium values of 0.9 ± 0.2 TU. Hence, baseflow in streams at higher elevations reflects a stronger influence from recent rainfall. Spring samples show lower overall tritium activity, averaging 1.0 ± 0.4 TU. In particular, the low-elevation springs Mbumbunyi and Mwangoto display the lowest tritium values, at 0.5 TU and 0.7 TU, respectively. Highland springs (Mwamkusa, Mandumu, Mkalokalo, and Moda Ghwa Mburi) show higher tritium values as compared to the low-elevation springs, with an average of 1.3 ± 0.2 TU (Fig. 10).

Fig. 11 presents the backward decay curves of tritium activity for both spring water and precipitation, assuming exponential radioactive decay. These curves represent the tritium activity that the sampled water would have had historically. Indicative apparent residence time is estimated graphically from the intersection between the decay curve of a spring and the corresponding precipitation curve (see Section 3.5 for details). Highland springs (Mkalokalo, Mandumu, and Mwamkusa) have current tritium values lower than those of present-day highland rainfall and streams. Given that tritium in rainfall is assumed to be constant since 2010 (see Section 3.5), highland springs show the signature of modern rainfall, likely indicating multi-year apparent residence times. The transition-zone and lowland springs (Mwangoto and Mbumbunyi, respectively), emerging approximately 600 m below the highland springs, show lower tritium values than both the highland springs and highland rainfall. This lower tritium activity could indicate a smaller contribution of modern recharge and longer, potentially decadal apparent residence times. It is worth noting that the latter springs may also be reflecting a mixed signal of highland and lowland infiltrated rainwater.

Fig. 10 illustrates a clear inverse relationship between tritium activity and bicarbonate, with lower tritium values generally associated with higher bicarbonate. In general, older groundwater is expected to have both lower tritium activity and higher bicarbonate. Fig. 10 and Fig. 11 show a transition from relatively young, weakly mineralized groundwater at higher elevations to older, more mineralized groundwater at lower elevations.

5. Discussion

5.1. Controls on rainfall partitioning and recharge

Large spatial gradients in precipitation are common in mountainous catchments (Anders et al., 2006; Prat and Barros, 2010; Giambelluca et al., 2013), with slope exposure having a greater impact on rainfall than mean elevation in East Africa (Oettli and Camberlin, 2005). The decrease in rainwater chloride from the lowlands toward the inland highlands, consistent with Kretchy's (2014) findings in a tropical highland-lowland system in Ghana, can be attributed to the progressive fallout of marine aerosols as the air masses move inland (Junge and Werby, 1958). In the Taita Hills, rainfall amount and chloride concentration gradients appear to be inversely related, consistent with the dilution hypothesis and possibly also reflecting enhanced fog interception (occult precipitation) in the highlands. Since the chloride gradient was derived from rainfall-weighted means, it is not independent of rainfall amount; however, the same pattern was also obtained using arithmetic mean chloride concentrations. Although denser tree canopies can enhance dry deposition (Deng et al., 2013), higher chloride

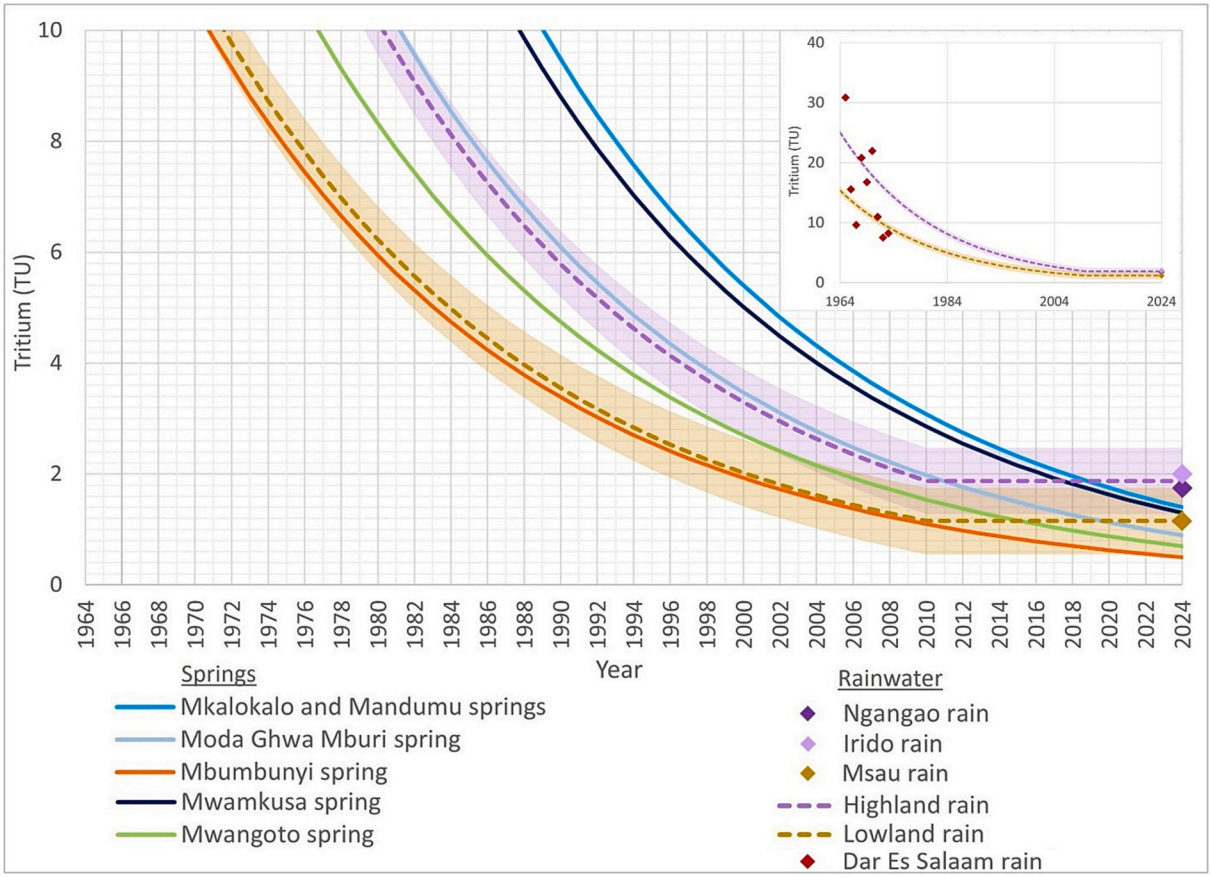


Fig. 11. Backward reconstruction of tritium activity (TU) in springs and rainwater using tritium measurements from 2024. Shaded bands represent uncertainty ranges associated with modern rainwater tritium composition. Note: the tritium level in precipitation was assumed to be constant from 2010 to 2024.

concentrations were observed in open, bulk rainfall samples from the relatively less forested lowlands of the Taita Hills. This suggests that topography may have a stronger influence on measured rainwater chloride values than land cover. Another factor could be that bulk rainwater collectors capture only part of the dry deposition, a common issue as reported by Michelsen et al. (2024).

Mkaya (2013) developed a SWAT model using historical data from the Wundanyi catchment and found an average runoff coefficient of only 7%, but an average actual evapotranspiration of 75% of total rainfall for the period 1975-2004, in line with the findings presented in Section 4.5. However, the water balance reported by Mkaya (2013) for the Wundanyi catchment appeared not to close fully. For 2023 and 2024, the annual water balance of the Wundanyi catchment was largely closed, whereas a negative residual was estimated for 2025. This imbalance may reflect actual changes in storage or uncertainties in water balance components. Longer-term monitoring is required to better assess hydrological variability and potential trends in the Wundanyi catchment.

Employing multiple recharge estimation approaches is essential for a more reliable assessment. Abiye (2016) found that baseflow separation methods were generally inconsistent with most recharge estimation techniques. At the Wundanyi catchment scale, natural groundwater recharge estimated from rainfall partitioning is comparable to the sum of baseflow and estimated abstractions. Despite this interesting consistency, estimating groundwater recharge from streamflow recession curves remains uncertain, particularly in catchments affected by anthropogenic activity (Fetter, 2001). In contrast, results are less consistent at the subcatchment scale due to the influence of lateral subsurface flows across subcatchments on baseflow (Table 1). This also suggests that heterogeneities in fractured rock environments exert a stronger influence at smaller spatial scales, whereas larger-scale analyses integrate local variability and consequently converge toward more consistent results, as also concluded by Jiménez-Martínez et al. (2013).

Groundwater recharge derived from the chloride mass balance (CMB), not affected by abstractions, is compared with recharge estimated from the rainfall partitioning under natural conditions at both the catchment and subcatchment scales (Fig. 12). The CMB-derived recharge values are consistently lower than those derived from rainfall partitioning. At the Wundanyi catchment scale, the average rainwater Cl required to obtain the same CMB-derived recharge values as those obtained with the rainfall partitioning would be 2.3 mg/L. However, the average measured rainwater Cl at Wundanyi is only about 1.5 mg/L.

Occult precipitation may be an important additional contribution to water balance inputs in highland forests (Erdogan et al., 2011; Hohenthal et al., 2015). Considerable contributions of fog deposition to groundwater recharge in northern Kenya mountain systems were reported by Ingraham and Matthews (1988). In the forested mountains of the Taita Hills, additional inputs from fog deposition of around 20% have been reported by the University of Helsinki (2024). However, significant portions of water inputs from occult precipitation may be lost through direct evaporation from the canopy (Edwards et al., 1983). Makowski-Giannoni et al. (2016) reported that chloride concentrations in occult precipitation were 1.35 times those in rainwater. Disregarding occult precipitation, as in our study, could therefore lead to an underestimation of groundwater recharge in the highlands, particularly in forested areas. Wundanyi's rainwater Cl concentration would increase to only 1.6 mg/L (< 2.3 mg/L) if occult precipitation equivalent to 20% of total precipitation, with a Cl concentration of 2 mg/L, is added to the rainfall input. Therefore, adding occult precipitation is insufficient to explain the difference between the recharge values derived from the

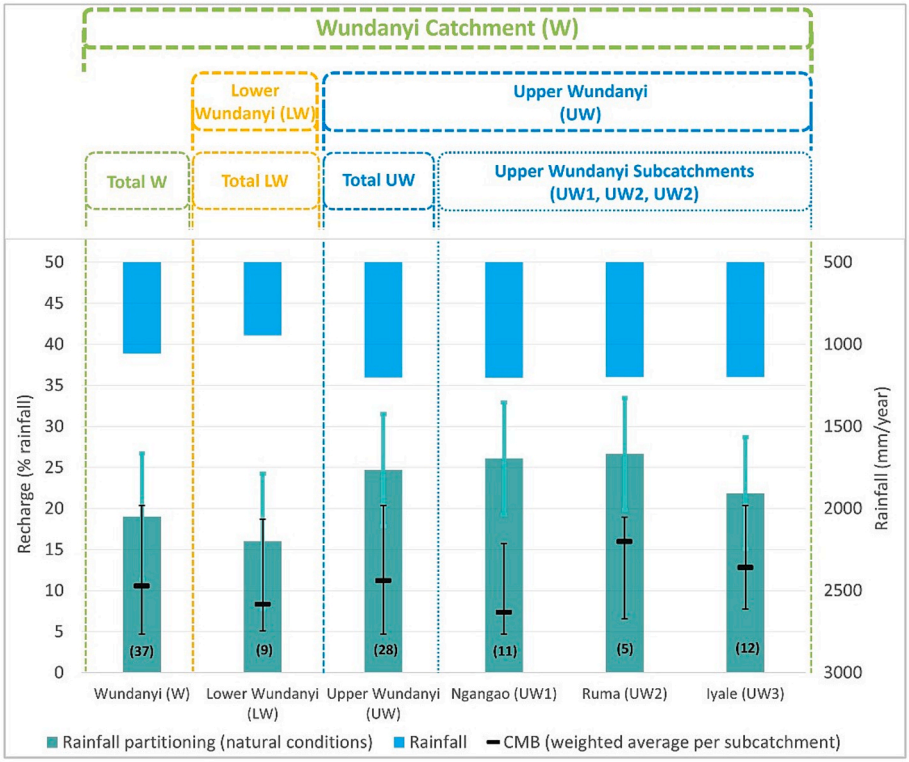


Fig. 12. Comparison of natural recharge values across the Wundanyi catchment and subcatchments, shown alongside total annual rainfall for 2024. Thin green vertical bars indicate the sensitivity of rainfall partitioning-derived recharge to ±10% variations in ET_a. Thin black vertical bars represent the minimum and maximum CMB-derived values.

CMB and rainfall partitioning. However, the complex dynamics between occult precipitation, rainfall, interception, infiltration, evapotranspiration, and groundwater recharge require further investigation.

The reliability of CMB-derived recharge estimates depends largely on the quantification of total atmospheric chloride input to the system (Michelsen et al., 2024), which can be particularly challenging in forested catchments. Although the permanently exposed bulk collectors likely captured part of the dry deposition, the difference between the measured average rainwater chloride at Wundanyi and the concentration required for the CMB-derived recharge to match the rainfall-partitioning estimate suggests that dry deposition was not fully captured, particularly in forested areas. Vet et al. (2014) reported that dry deposition globally equals or exceeds wet deposition, even over continental margins. However, direct measurements of dry deposition remain sparse, challenging, and uncertain (Wesely and Hicks, 2000). More local studies, such as Deng et al. (2013), showed that chloride deposition in a coastal forest in South Australia was 28% higher in eucalyptus-dominated areas and 89% higher in pine-dominated areas than in open areas. Data reported by Laclau et al. (2005) also show that total chloride input beneath eucalyptus canopies can be approximately 1.5 times higher than that from open rainfall during the rainy season. Svensson et al. (2012), based on a synthesis of 32 catchments across Europe and North America, showed that dry deposition can contribute 15 to 75% of total chloride input in forest catchments, with a mean contribution of 43%. In a Mexican tropical montane landscape, Ponette-González et al. (2010) similarly found that chloride inputs under forest and agroforest canopies were higher than those measured in collectors in open or cleared areas. Interestingly, the largest difference between the recharge values derived from the CMB and rainfall partitioning is observed in Ngangao, the most forested subcatchment (Fig. 12), which may reflect a larger unaccounted contribution of dry deposition than in the other subcatchments. Another possible explanation is that the sampled springs in Ngangao may predominantly represent the shallow flow system, which is more affected by evapotranspiration, resulting in relatively higher chloride concentrations and lower CMB-derived recharge values. In fact, part of the recharge generated within Ngangao flows toward the southern Upper Wundanyi subcatchments, as indicated in Sections 4.4 and 4.5.

At the Wundanyi catchment scale, the relative difference between the measured average rainwater Cl (1.5 mg/L) and the concentration required for the CMB values to match those from rainfall partitioning (2.3 mg/L) is approximately 50%, which is broadly consistent with the range reported in the aforementioned literature.

On a global scale, Mohan et al. (2018) found that land cover and meteorological factors had the strongest influence on groundwater recharge. In the Taita Hills, both the CMB and rainfall partitioning methods show higher actual groundwater recharge in the highlands and Upper Wundanyi subcatchments. This consistent pattern likely reflects the greater precipitation inputs in the highlands. However, the multivariable regression analysis, using the CMB-derived recharge ratios, showed that, among the tested variables, recharge ratio variability is more strongly associated with vegetation type than with dominant lithology, elevation, slope steepness, or proximity to lineaments. This observation should be interpreted cautiously because the overall multivariable model was not statistically significant. Moreover, the larger apparent influence of vegetation type may be amplified by the potentially underestimated CMB-derived recharge ratios at Ngangao. Overall, the multivariable regression analysis could be further strengthened by reliable, site-specific data on soil thickness and geological structures.

Rainfall partitioning showed that the average recharge ratio in the forested subcatchments (i.e., Upper Wundanyi) is approximately 25% of rainfall, about 1.5 times higher than in the thicket-dominated subcatchments of Lower Wundanyi and Dembwa. Cardwell (2017) highlighted that infiltration rates in forest soils of the Taita Hills were higher than those in cultivated and grazing lands. Etukutan (2024) also

reported higher infiltration rates in montane (196 ± 81 cm/h) and plantation (71 ± 9 cm/h) forests compared to agroforestry (54 ± 42 cm/h) and thicket (44 ± 13 cm/h) (Table S5).

5.2. Discharge dynamics and subsurface connectivity

Many springs, especially those emerging in the highlands of the Taita Hills, showed limited sensitivity to seasonality. Cardozo (2022) found that springs of the Wundanyi and Mwatate catchments were mostly resilient to droughts, with the most resilient springs being at elevations of 1350 to 1700 m AMSL. This limited seasonal variability reflects relatively large groundwater storage, at least in the spring recharge areas. In the Taita Hills, underlain by metamorphic gneiss, Khan (2022) interpreted groundwater flow paths toward discharge areas as being associated with fractures, faults, and dikes, with smaller, shallower flow systems occurring in the weathered zone.

The much larger stream discharge compared to the combined discharge of all mapped springs indicates that a substantial portion of streamflow is supplied by shallow subsurface stormflow (interflow) and, more importantly, by baseflow draining the weathered and fractured zones. Mul et al. (2007) studied a gneiss-dominated highland-lowland system in Tanzania and similarly reported that springs contributed less than 5% of the catchment's total discharge.

In the Wundanyi catchment, the rapid streamflow response to rainfall events, mainly associated with the stormflow component, is likely related to the steep topography since infiltration rates reported by Etukutan (2024) indicate very rapid infiltration. River abstractions are expected to have a relatively limited influence on stormflow, as they predominantly affect the river baseflow. The calculated median recession constants for the studied catchments and subcatchments (0.94 to 0.96) fall within the range typically associated with baseflow-dominated systems (Pilgrim and Cordery, 1992).

Geological structures may act as flow conduits, barriers, or combined conduit-barrier systems (Caine et al., 1996), making it crucial to understand their role, especially in geologically complex study areas (Freeze and Cherry, 1979).

In the Taita Hills, geological structures appeared to facilitate subsurface flow. In particular, lineaments are likely to facilitate subsurface water transfer between subcatchments, as the central-western subcatchments in the study area (i.e., southwestern subcatchments of the Wundanyi catchment) showed the highest specific discharge. This is also reflected in the calculated lateral subsurface flows (Table 1). Moreover, several high-discharge springs occurred within these subcatchments, further supporting the presence of a well-developed fracture network. Previous studies have also indicated that active faults can largely control subsurface flow in hard-rock terrains (Barton et al., 1995; Gudmundsson, 2000; Gudmundsson et al., 2001). In particular, mapped structures in the Taita Hills were previously interpreted as potential preferential flow pathways (Pohl and Niedermayr, 1979; Pohl et al., 1980). Groundwater level monitoring across structures, tracer tests, and geophysical surveys could help assess the hydraulic function of individual lineaments.

5.3. Evidence of groundwater flow paths and relative residence times

The observed strong seasonal stability of bicarbonate and major ion composition further suggests that the system is largely groundwater-dominated. Surface water at the outlet of the Wundanyi catchment had lower bicarbonate concentrations during the wet season, possibly due to dilution from overland flow and shallow subsurface flow (interflow). In the headwaters, dilution effects are less evident since bicarbonate and mineralization are already low.

Water chemistry in the study area is governed by the weathering of metamorphic silicate rocks, mainly gneiss. Most groundwater samples clustered within the silicate weathering domain, together with the coupled increase in bicarbonate and dissolved silica, further indicating that silicate weathering is the dominant geochemical process. For instance, the weathering reaction of albite to kaolinite can be expressed as (Appelo and Postma, 2004) :

$$2Na(AlSi_3)O_8 + 2H^+ + 9H_2O \rightarrow Al_2Si_2O_5(OH)_4 + 2Na^+ + 4H_4SiO_4 \quad (7)$$

$$CO_2 + H_2O \rightleftharpoons H^+ + HCO_3^-$$

Combining these reactions gives:

$$2Na(AlSi_3)O_8 + 2CO_2 + 11H_2O \rightarrow Al_2Si_2O_5(OH)_4 + 4H_4SiO_4 + 2Na^+ + 2HCO_3^- \quad (8)$$

Silicate weathering was also found to be the dominant geochemical process by Mul et al. (2007) in a gneiss-dominated highland-lowland system. Lowland and some transition-zone samples plotted at higher bicarbonate and silica values, indicating more advanced water-rock interactions and weathering. In particular, elevated dry-season bicarbonate values at the outlets of the Wundanyi and Mwatate catchments suggest that older, more mineralized groundwater flow systems dominate. Khan (2022) found that high-bicarbonate springs in the Taita Hills usually reflect a deeper flow system, as indicated by higher Ca/Sr ratios. Mul et al. (2007) also found that mineralization increased with decreasing altitude in the metamorphic rock highland-lowland system they studied.

The Wundanyi River baseflow changed its behavior along its course, receiving older water, as reflected by decreasing tritium values and increasing alkalinity and silica concentrations, particularly at Mwangoto and further downstream at the catchment outlet at Msau. Spring samples showed lower overall tritium levels than surface water, reflecting longer residence times and greater mixing with older groundwater. According to the classification by Clark and Fritz (2013), the tritium values measured in the sampled springs reflect a mixture of old and recent recharge. Lower tritium values were also generally associated with higher bicarbonate, reflecting a transition from relatively young, poorly mineralized groundwater at higher elevations to older, more mineralized groundwater at lower elevations, consistent with deeper, longer groundwater flow paths in both the transition zone and the lowlands.

In summary, the relatively low mineralization and higher tritium activities at higher elevations are consistent with recharge areas characterized by shorter and shallower groundwater flow paths. The downslope increases in EC, HCO_3^-, silica, accompanied by a decrease in tritium activities, indicate longer flow paths, more advanced water-rock interaction, and discharge in the transition zone and lowlands. The higher mineralization of lowland wells (Fig. 9) points towards limited regional subsurface freshwater flow and mixing with local resident water with much lower rainfall and recharge rates, consistent with observations from a highland-lowland system in Ethiopia (Mechal et al., 2016).

5.4. Conceptual model

In line with the main goal of this study, the complementary hydrological, hydrochemical, isotopic, structural, and spatiotemporal lines of evidence were integrated to develop a data-driven conceptual model of the Taita Hills water tower system. Fig. 13 illustrates the key hydrological processes, fluxes, and physical features of this model.

Overall, the studied system is characterized by substantial rainfall and fog capturing in the highlands, as well as by the groundwater storage and streamflow regulation functions typically associated with natural water towers (Messerli et al., 2004; Immerzeel et al., 2020). The combined evidence indicates hydrological connectivity between the highlands and lowlands. Topography and slope exposure are key drivers of rainfall distribution and actual recharge; vegetation type appears to have a greater influence on spatial recharge variability than lithology and slope steepness; and structural geology probably influences flow distribution through preferential pathways.

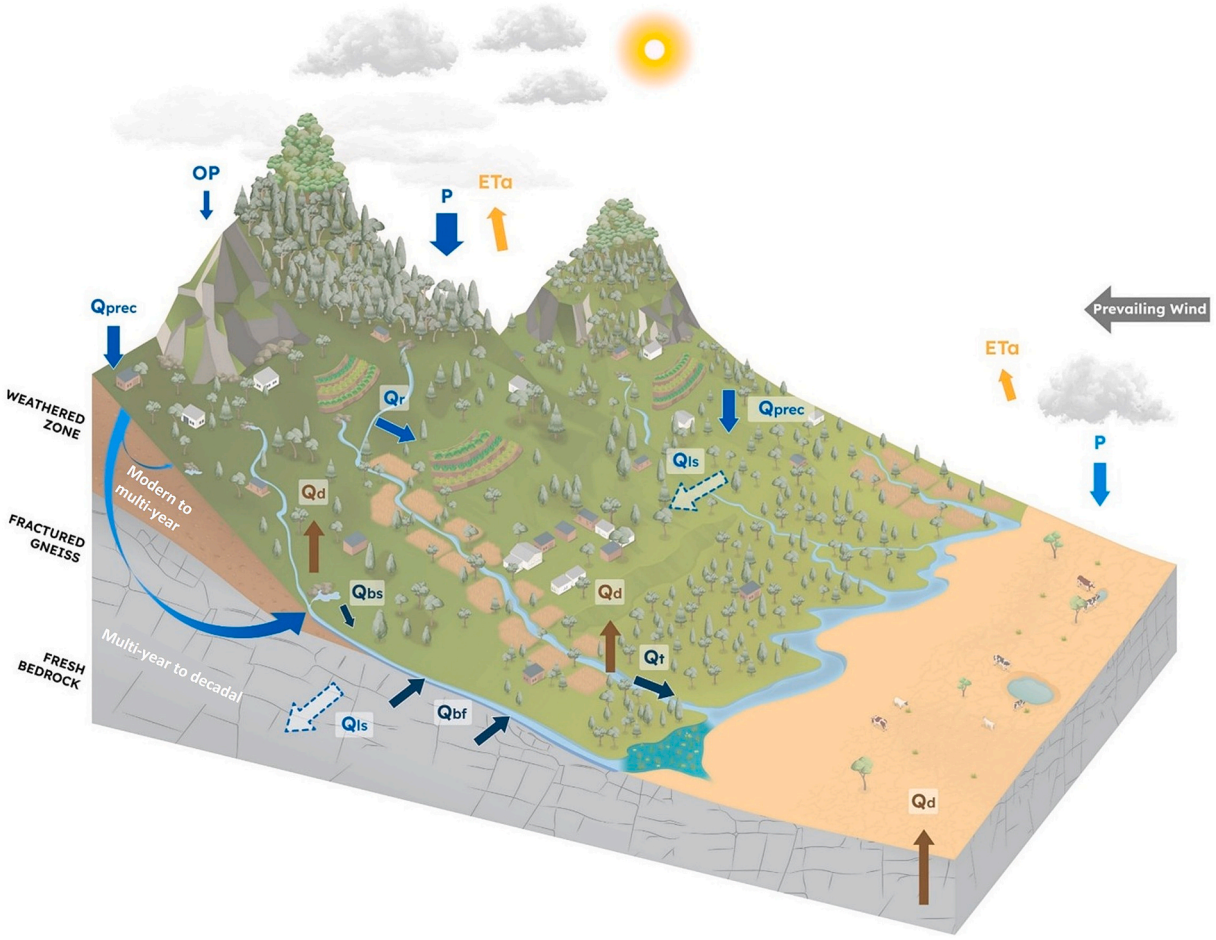


Fig. 13. Conceptual model of the Taita Hills highland-lowland system illustrating key hydrological processes, fluxes, and physical features. The model illustrates orographic precipitation (P), occult precipitation (OP), evapotranspiration (ET_a), stormflow (Q_r), spring-fed baseflow (Q_{bs}), fracture-fed baseflow (Q_{bf}), total discharge (Q_t), groundwater recharge (Q_{prec}), subsurface lateral flows (Q_{ls}) and abstractions from multiple sources (Q_d).

In particular, the highlands, which receive significant rainfall and occult precipitation, are characterized by higher groundwater recharge and disproportionately larger total runoff than the surrounding lowlands, consistent with the findings of Messerli et al. (2004) and Viviroli et al. (2007). As a result, the highlands serve as the principal zone of precipitation input to the system. Local observations indicate significant declines in spring and stream discharge over recent decades (Hohenthal et al., 2015), suggesting that lowland baseflow contributions may have been larger or more persistent in the past.

The estimated multi-year residence times indicate considerable storage capacity. The high baseflow proportion of streamflow and the perennial behavior of most springs and streams indicate an important groundwater-buffering function, consistent with findings of Bruijnzeel (2004) and Somers and McKenzie (2020). In addition, the limited seasonal variation in recharge ratios suggests that recharge is integrated over multiple years rather than short-term inputs. These observations suggest that groundwater storage and baseflow still play a key role in sustaining dry-season flows.

The progressive groundwater mineralization and decreasing tritium activities from the highlands toward the lowlands reflect a systematic downslope evolution of groundwater flow paths and longer relative residence times. These and other lines of evidence show that the study area features two types of flow systems: a local system with young water, mostly flowing through weathered material and shallow fractures, and a subregional, intermediate flow system with older (decadal scale) water, flowing through fractured gneiss.

Unlike cryospheric water towers, where snow and glacier storage and subsequent melt contribute substantially to the regulation and seasonal release of water (Immerzeel et al., 2020), these results indicate that the Taita Hills function as a groundwater-dominated water tower system, with spatially heterogeneous recharge, flow influenced by preferential subsurface pathways associated with geological structures, and buffered discharge. In particular, the spatial correspondence between high specific discharge, high spring discharge, elevated spring density, and lineament orientation suggests that structural geology has an important influence on groundwater flow paths, discharge mechanisms, and thereby the system's regulation function. This interpretation is consistent with earlier hydrogeological observations by Pohl and Niedermayr (1979) that groundwater in the metamorphic rocks of the Taita Hills occurs mainly in fissures and fractures.

5.5. *Uncertainties, limitations and future work*

This study integrates surface hydrology, recharge and water-balance calculations, hydrochemistry, isotopes, and geospatial mapping to assess the interlinked functions of tropical, hard-rock water tower systems. However, uncertainties in rainwater chloride inputs and dry deposition, baseflow separation methods and parameters, rating-curve extrapolation, estimates of actual water withdrawals and return flows, residence time interpretation, and the hydraulic role of geological structures could affect some interpretations.

In particular, estimated stream peak flows were less certain than low- and intermediate-flow estimates because the highest recorded stages exceeded the gauged ranges. Except for the Ruma Stream, the sensitivity

analysis indicated that extrapolating the rating curves beyond their gauged stage ranges had a limited effect on total discharge. Additional high-flow measurements would, however, improve future discharge estimates. The differencing approach used to estimate discharge from Ngangao and Iyale combines uncertainties from the contributing discharge records, making these estimates less certain than directly monitored discharge. Installation of pressure transducers at the Ngangao and Iyale outlets is therefore recommended; this was not feasible during the monitoring period because no suitable and secure installation locations could be identified near the outlets.

Baseflow estimates depend on the separation method, parameter selection in parameter-based methods, and subjectivity in defining the baseflow-stormflow boundary in graphical methods (Nathan and McMahon, 1990; Pelletier and Andréassian, 2020). Therefore, reporting the sensitivity range is more cautious and transparent than reporting a single BFI value. Excluding the two extremes, BFI values range from 61% to 78% across all tested methods and parameter combinations. Nevertheless, the agreement between the adopted Eckhardt result and the graphical methods supports the overall interpretation and key conclusions.

Moreover, cross-subcatchment groundwater transfers may affect the partitioning of discharge among Ruma, Iyale, and Ngangao, but are expected to have less influence on the aggregated Upper Wundanyi contribution since the most significant transfers occur among these subcatchments. Negligible changes in storage do not necessarily imply the absence of a lag effect in the annual water balance. In fact, the multi-year groundwater residence times indicate that streamflow, particularly baseflow, integrates recharge from preceding years. An additional source of uncertainty would be the actual river water abstractions, which were assumed to be equal to the calculated water demand. The demand estimates are themselves uncertain because they depend on assumed water-use rates. Unquantified return flows may also affect the recharge estimates and water balance calculations.

The subcatchment-averaged CMB-derived recharge values showed limited sensitivity to the selected discharge-class weights, with relative differences remaining below 5% (Fig. S12). However, CMB-derived recharge values remain sensitive to the rainwater chloride concentrations; existing bulk rainwater collectors should be complemented with throughfall measurements to better estimate total atmospheric chloride inputs and enhance the reliability of the CMB-derived results.

Future work should prioritize continuous groundwater level and spring discharge monitoring, peak-flow gauging in streams, tracer and hydraulic testing across geological structures, geophysical surveys, throughfall chloride measurements, and longer-term isotope and hydrometeorological monitoring. Where sufficient data become available, updated observations could support numerical modeling to better assess the drivers of change and explore system responses under changing land and climate conditions, including interannual hydroclimatic variability. This is particularly relevant as local communities have reported substantial declines in spring and stream discharge over recent decades (Hohenthal et al., 2015).

6. Conclusions

The hydrological value of the highlands in the Taita Hills is significant, as these areas provide considerable amounts of water both locally and to the lowlands through the transition zone. However, this study highlighted that the hydrological functioning of water tower systems cannot be assessed from topography or surface hydrological observations alone; potential structural controls, groundwater flow systems, and land cover, particularly vegetation type, should also be considered. The findings also highlight the role of groundwater as a key buffer in highland-lowland systems, helping to regulate freshwater availability during periods of increased hydroclimatic variability, including prolonged droughts. For instance, ecological restoration and terracing could enhance groundwater recharge and, given the potentially important role of faults and fractures, may thereby help sustain baseflow and potentially restore it to levels closer to those observed in previous decades.

While the relative importance of the dominant processes in this study will likely vary among fractured tropical mountain systems, the mechanisms identified here provide a useful basis for understanding the functioning of other hard-rock highland-lowland systems. As mountainous regions become increasingly important in demographic, agricultural, and political processes, a sound understanding of the functioning of highland-lowland systems will be essential for informing land and water management and adaptation planning. In particular, initiatives aimed at enhancing water retention capacity and water availability in these fragile systems should be undertaken, given the direct impacts experienced by local communities, such as declines in spring and stream discharge.

CRediT authorship contribution statement

Michel R. Frem: Writing – original draft, Writing – review & editing, Conceptualization, Data curation, Formal analysis, Investigation, Methodology, Visualization. **Tibor Y. Stigter:** Writing – review & editing, Supervision, Project administration, Methodology, Investigation, Funding acquisition, Formal analysis, Conceptualization. **Boris M. van Breukelen:** Writing – review & editing, Supervision, Methodology, Conceptualization. **Gretchen M. Gettel:** Supervision, Project administration, Funding acquisition. **Graham P. W. Jewitt:** Supervision. **Benson Mwakachola:** Investigation.

Declaration of competing interest

The authors declare the following financial interests/personal relationships which may be considered as potential competing interests: Michel Frem reports financial support was provided by European Union. Michel Frem reports financial support was provided by Netherlands Ministry of Foreign Affairs. Michel Frem reports administrative support was provided by University of Helsinki. The other authors declare that they have no known competing financial interests or personal relationships that could have appeared to influence the work reported in this paper.

Acknowledgements

The authors acknowledge the support from colleagues at the Taita Research Station, including Petri Pellikka, Mwadime Jomba, Julius Omondi and James Mwangombe, and from multiple community members. The authors acknowledge the knowledge generated by various researchers who worked in the area, most of whom were cited in this manuscript. The authors also acknowledge the support and effort of various field assistants. We thank Dejan Cuturilov (Mapversum) for the design of the graphical abstract based on the authors' original conceptual sketch.

Appendix A. Symbols, meanings and indicative units

Table A.1
Symbols, meanings and indicative units.

Symbol	Meaning	Unit[1]
C(t)	Tritium activity after an elapsed time t	TU
C_0	Tritium activity at the time of recharge	TU
t	Time elapsed since recharge	y
$T_{1/2}$	Tritium half-life	y
λ	Radioactive decay constant of tritium	1/y
P	Precipitation	mm/y
Q_{prec}	Groundwater recharge	mm/y
S_{root}	Water stored or released in the root zone	mm/y
D_d	Dry atmospheric chloride deposition	mg/(m^2.y)
Cl_P	Chloride concentration in precipitation	mg/L
Cl_{Qr}	Chloride concentration in stormflow	mg/L
Cl_{Qprec}	Chloride concentration in percolating groundwater	mg/L
Cl_{Sroot}	Chloride concentration in root-zone water	mg/L
C_r	Runoff coefficient	-
A	(Sub)catchment area	km^2
N	Duration of stormflow following a storm event	d
Q_b	Baseflow	mm/y
Q_t	Total streamflow	mm/y
Q_r	Stormflow	mm/y
α	Recession constant	-
BFI_{max}	Maximum long-term baseflow index parameter	-
ET_a	Actual evapotranspiration	mm/y
ΔS	Change in catchment water storage	mm/y
Q_{ls}	Net lateral subsurface flow	mm/y
Q_d	River abstractions	mm/y
C_{UW}	Upper Wundanyi contribution to Wundanyi streamflow	%
$Q_{t,UW}$	Mean Upper Wundanyi streamflow	m^3/d
$Q_{t,W}$	Mean Wundanyi streamflow	m^3/d

[1] Units listed are indicative of those used in the manuscript and related figures. Unit conversions were applied consistently where required.

Appendix B. Supplementary data

Supplementary data to this article can be found online at https://doi.org/10.1016/j.jhydrol.2026.136595.

Data availability

Data are still being used as part of an ongoing PhD project. Upon completion, data will be made available on request, noting that hydro-meteorological data obtained from third parties are subject to the data-sharing conditions of the respective providers.

References

Abatzoglou, J.T., Dobrowski, S.Z., Parks, S.A., Hegewisch, K.C., 2018. Terraclimate, a high-resolution global dataset of monthly climate and climatic water balance from 1958-2015. Sci. Data 5, 170191.

Abera, T.A., Vuorinne, I., Munyao, M., Pellikka, P.K., Heiskanen, J., 2022. Land cover map for multifunctional landscapes of Taita Taveta County, Kenya, based on Sentinel-1 radar, Sentinel-2 optical, and topoclimatic data. Data 7 (3), 36.

Abiye, T., 2016. Synthesis on groundwater recharge in Southern Africa: a supporting tool for groundwater users. Groundw. Sustain. Dev. 2, 182–189.

Adler C, Wester P, Bhatt I, Huggel C, Insarov GE, Morecroft MD, Muccione V, Prakash A (2022) Cross-Chapter Paper 5: Mountains. In: Climate Change 2022: Impacts, Adaptation and Vulnerability. Contribution of Working Group II to the Sixth Assessment Report of the Intergovernmental Panel on Climate Change, pp. 2273-2318. Cambridge University Press, 2023.

Adloff M, Singer MB, MacLeod DA, Michaelides K, Mehrnegar N, Hansford E, Funk C, Mitchell D (2022) Sustained water storage in Horn of Africa drylands dominated by seasonal rainfall extremes. Geophysical Research Letters, 49(21), p.e2022GL099299.

Afullo, A.O., Danga, B.O., Odhiambo, F., 2014. Implications of time to water source on water use in the arid and semi-arid land counties of Kenya. Int. J. Water 8 (4), 381–400.

Alcalá, F.J., Custodio, E., 2008. Atmospheric chloride deposition in continental Spain. Hydrol. Process. 22 (18), 3636–3650.

Alweny S, Nsengiyumva P, Gatarabirwa W (2014) Africa Sustainable Mountain Development Technical Report No. 1. Kampala/Cambridge, UK, Albertine Rift Conservation Society (ARCOS).

Anders, A.M., Roe, G.H., Hallet, B., Montgomery, D.R., Finnegan, N.J., Putkonen, J., 2006. Spatial patterns of precipitation and topography in the Himalaya. Spec. Pap. Geol. Soc. Amer. 389, 39–53.

Appelo, C.A.J., Postma, D., 2004. Geochemistry, Groundwater and Pollution. Balkema, Leiden, The Netherlands.

Barnett, T.P., Pierce, D.W., Hidalgo, H.G., Bonfil, C., Santer, B.D., Das, T., Bala, G., Wood, A.W., Nozawa, T., Mirin, A.A., Cayan, D.R., 2008. Human-induced changes in the hydrology of the western United States. Science 319 (5866), 1080–1083.

Barton, C.A., Zoback, M.D., Moos, D., 1995. Fluid flow along potentially active faults in crystalline rock. Geology 23, 683–686.

Beentje HJ, Ndiang'ui N (1988) An ecological and floristical study of the forests of the Taita Hills, Kenya: Ecology of the Forests. Utafiti: occasional papers of the National Museums of Kenya 1(2), 23–42.

Borghesio, L., Samba, D., Githiru, M., Bennun, L., Norris, K.E.N., 2010. Population estimates and habitat use by the Critically Endangered Taita Apalis Apalis fuscigularis in south-eastern Kenya. Bird Conserv. Int. 20 (4), 440–455.

Bruijnzeel, L.A., 2001. Hydrology of tropical montane cloud forests: a reassessment. Land Use and Water Resour. Res. 1, 1, 1732–2016-140258.

Bruijnzeel, L.A., 2004. Hydrological functions of tropical forests: not seeing the soil for the trees? Agric. Ecosyst. Environ. 104, 185–228.

Caine, J.S., Evans, J.P., Forster, C.B., 1996. Fault zone architecture and permeability structure. Geology 24 (11), 1025–1028.

Cardozo, D.R., 2022. Assessment of the spring resilience to drought under different land use type in Taita Hills, Kenya. IHE Delft Institute for Water Education, Delft, the Netherlands.

Cardwell, A., 2017. The effect of land use on infiltration in Taita hills, Kenya. University of Helsinki. Master's thesis.

Clark, B.J., Pellikka, P.K., 2009. Landscape analysis using multi-scale segmentation and object-oriented classification. In: Recent Advances in Remote Sensing and Geoinformation Processing for Land Degradation Assessment. Taylor & Francis Group, London, pp. 323–342.

Clark, I.D., Fritz, P., 2013. Environmental Isotopes in hydrogeology. CRC Press.

Danielescu, S., MacQuarrie, K.T.B., Popa, A., 2018. SEPHYDRO: a customizable online tool for hydrograph separation. Groundwater 56, 589–593.

Deng, Z., Priestley, S.C., Guan, H., Love, A.J., Simmons, C.T., 2013. Canopy enhanced chloride deposition in coastal South Australia and its application for the chloride mass balance method. J. Hydrol. 497, 62–70.

East African Meteorological Department, 1966. Monthly and annual rainfall in Kenya during the 30 years, 1931 to 1960. East African Common Services Organization, Nairobi.
Eckhardt, K., 2005. How to construct recursive digital filters for baseflow separation. Hydrol. Process. 19, 507–515.
Eckhardt, K., 2012. Analytical sensitivity analysis of a two parameter recursive digital baseflow separation filter. Hydrol. Earth Syst. Sci. 16 (2), 451–455.
Edwards, K.A., Classen, G.A., Schroten, E.H.J., 1983. The water resource in tropical Africa and its exploitation (Vol. 6). ILRI.
Erdogan, H.E., Pellikka, P.K., Clark, B.J., 2011. Modelling the impact of land-cover change on potential soil loss in the Taita Hills, Kenya, between 1987 and 2003 using remote-sensing and geospatial data. Int. J. Remote Sens. 32 (21), 5919–5945.
Eriksson, E., Khunakasem, V., 1969. Chloride concentrations in groundwater, recharge rate and rate of deposition of chloride in the Israel coastal plain. J. Hydrol. 7, 178–197.
Etukutan, P.E., 2024. Assessing the relationship between groundwater recharge and discharge in a natural water tower system in Wundanyi catchment, Taita Hills – Kenya. IHE Delft Institute for Water Education, Delft, the Netherlands.
Ferrer, N., Folch, A., Lane, M., Olago, D., Odida, J., Custodio, E., 2019. Groundwater hydrodynamics of an Eastern Africa coastal aquifer, including La Niña 2016–17 drought. Sci. Total Environ. 661, 575–597.
Fetter, C.W., 2001. Applied Hydrogeology, 4th ed. Prentice Hall, Upper Saddle River.
Freeze, R.A., Cherry, J.A., 1979. Groundwater. Prentice-Hall, Englewood Cliffs, New Jersey, p. 604.
Giambelluca, T.W., Chen, Q., Frazier, A.G., Price, J.P., Chen, Y.L., Chu, P.S., Eischeid, J. K., Delparte, D.M., 2013. Online rainfall atlas of Hawaii. Bull. Amer. Meteor. Soc. 94, 313–316.
Gudmundsson, A., 2000. Active fault zones and groundwater flow. Geophys. Res. Lett. 27, 2993–2996.
Gudmundsson, A., Berg, S.S., Lyslo, K.B., Skurtveit, E., 2001. Fracture networks and fluid transport in active fault zones. J. Struct. Geol. 23, 343–353.
Hamilton LS, Cassells D (2003) Hydrology overview. In: Dudley N, Stolton S, editors. Running pure: the importance of forest protected areas to drinking water. Gland: World Bank/WWF Alliance for Forest Conservation and Sustainable Use.
Harris, C., Burgers, C., Miller, J., Rawoot, F., 2010. O-and H-isotope record of Cape Town rainfall from 1996 to 2008, and its application to recharge studies of Table Mountain groundwater, South Africa. S. Afr. J. Geol. 113 (1), 33–56.
Heikinheimo, V., 2015. Impact of land cover change on aboveground carbon stocks in the Taita Hills, Kenya. Master's Thesis, University of Helsinki, Helsinki, Finland, 2015.
Hilberg, S., 2016. Natural tracers in fractured hard-rock aquifers in the Austrian part of the Eastern Alps - previous approaches and future perspectives for hydrogeology in mountain regions. Hydrogeol. J. 24 (5), 1091–1105.
Hohenthal, J., Owidi, E., Minoia, P., Pellikka, P.K., 2015. Local assessment of changes in water-related ecosystem services and their management: DPASER conceptual model and its application in Taita Hills, Kenya. Int. J. Biodiversity Sci., Ecosyst. Serv. Manage. 11 (3), 225–238.
Horkel A, Nauta WJ, Niedermayr G, Okelo RE, Pohl W, Wachira JK (1979) Geology of the Taita Hills quadrangle (with a geological map 1:50,000). Kenya Geological Survey Report 101, Nairobi, Kenya.
Hughes, D.A., Jewitt, G., Mahé, G., Mazvimavi, D., Stisen, S., 2015. A review of aspects of hydrological sciences research in Africa over the past decade. Hydrol. Sci. J. 60 (11), 1865–1879.
Immerzeel, W.W., Lutz, A.F., Andrade, M., Bahl, A., Biemans, H., Bolch, T., Hyde, S., Brumby, S., Davies, B.J., Elmore, A.C., Emmer, A., 2020. Importance and vulnerability of the world's water towers. Nature 577 (7790), 364–369.
Ingraham, N.L., Matthews, R.A., 1988. Fog drip as a source of groundwater recharge in northern Kenya. Water Resour. Res. 24 (8), 1406–1410.
Jasechko, S., 2019. Global isotope hydrogeology - review. Rev. Geophys. 57 (3), 835–965.
Jiménez-Martínez, J., Longuevergne, L., Le Borgne, T., Davy, P., Russian, A., Bour, O., 2013. Temporal and spatial scaling of hydraulic response to recharge in fractured aquifers: Insights from a frequency domain analysis. Water Resour. Res. 49 (5), 3007–3023.
Junge, C.E., Werby, R.T., 1958. The concentration of chloride, sodium, potassium, calcium, and sulfate in rain water over the United States. J. Atmos. Sci. 15 (5), 417–425.
Kaistinen H, Kivikko T, Marttunen E, Potinkara M, Muukkonen P, Siljander M (2018) Taita Taveta geodatabase. In Creating, managing, and analysing geospatial data and databases in geographical themes (pp. 58-80). University of Helsinki, Faculty of Science, Department of Geosciences and Geography.
Kenya National Bureau of Statistics, 2015. Taita Taveta County Statistical Abstract 2015. Kenya National Bureau of Statistics, Nairobi, Kenya.
Kenya National Bureau of Statistics (2019) Kenya Population and Housing Census. Volume II: Distribution of population by administrative units. Nairobi, Kenya: Kenya National Bureau of Statistics.
Kenyan Ministry of Water and Irrigation (2005) Practice Manual for Water Supply Services in Kenya. Kenya-Belgium Study and Consultancy Fund.
Khan, A.N., 2022. Assessing the recharge areas and groundwater flow systems of the Taita Hill springs in Kenya. IHE Delft Institute for Water Education, Delft, the Netherlands.
Kivivuori, B., 2013. The local perception on changes in water availability and accessibility in the Taita Hills, Kenya. Helsingfors Universitet, Finland.
Kretchy, S.M., 2014. Chemical and Isotopic composition of rainwater in the coastal, forest and mountainous areas of Volta region of Ghana. University of Ghana. Doctoral dissertation.
Lachassagne, P., Dewandel, B., Wyns, R., 2021. Hydrogeology of weathered crystalline/hard-rock aquifers—guidelines for the operational survey and management of their groundwater resources. Hydrogeol. J. 29 (8), 2561–2594.
Laclau, J.P., Ranger, J., Deleporte, P., Nouvellon, Y., Saint-André, L., Marlet, S., Bouillet, J.P., 2005. Nutrient cycling in a clonal stand of Eucalyptus and an adjacent savanna ecosystem in Congo: 3. Input–output budgets and consequences for the sustainability of the plantations. For. Ecol. Manage. 210 (1–3), 375–391.
Lindsey BD, Jurgens BC, Belitz K (2019) Tritium as an Indicator of Modern, Mixed, and Premodern Groundwater Age (No. 2019–5090). US Geological Survey; USGS: Reston, VA, USA.
Liniger HP, Weingartner R, Grosjean M (1998) Mountains of the World: Water Towers for the 21st Century. A Contribution to Global Freshwater Management, Mt. Agenda, Dep. of Geogr., Univ. of Berne, Berne.
Maeda, E.E., Pellikka, P.K., Clark, B., Siljander, M., 2011. Prospective changes in irrigation water requirements caused by agricultural expansion and climate changes in the eastern arc mountains of Kenya. J. Environ. Manage. 92, 982–993.
Makowski-Giannoni, S., Trachte, K., Rollenbeck, R., Lehnert, L., Fuchs, J., Bendix, J., 2016. Atmospheric salt deposition in a tropical mountain rainforest at the eastern Andean slopes of south Ecuador–Pacific or Atlantic origin? Atmos. Chem. Phys. 16 (15), 10241–10261.
Mechal, A., Birk, S., Winkler, G., Wagner, T., Mogessie, A., 2016. Characterizing regional groundwater flow in the Ethiopian Rift: a multimodel approach applied to Gidabo River Basin. Austrian J. Earth Sci. 109 (1).
Messerli, B., 1983. Stability and instability of mountain ecosystems: introduction to a workshop sponsored by the. United Nations University. Mountain Research and Development, pp. 81–94.
Messerli B, Hurni H, Wolde-Semayat B, Tedla S, Ives JD, Wolde-Mariam M (1988) African Mountains and Highlands: Introduction and Resolutions. Mountain Research and Development 8, no. 2/3 (1988): 93–100.
Messerli, B., Viviroli, D., Weingartner, R., 2004. Mountains of the World: Vulnerable Water Towers for the 21st Century. AMBIO Special Report 13, 29–34.
Michelsen, N., Rezvani, M., Schulz, S., 2024. Do you consider dry deposition in your chloride mass balance to estimate groundwater recharge? Yes, no, maybe. Hydrogeol. J. 32 (1), 31–36.
Mkaya, D.M., 2013. Evaluation of the impact of land use change on catchment hydrology: The case of Wundanyi River catchment in Taita Hills, Kenya. Egerton University. MSc thesis.
MoEaM (Ministry of Environment and Mineral Resources) (2013) Environment action plan. Ministry of Environment and Mineral Resources, Republic of Kenya.
Mohan, C., Western, A.W., Wei, Y., Saft, M., 2018. Predicting groundwater recharge for varying land cover and climate conditions–a global meta-study. Hydrol. Earth Syst. Sci. 22 (5), 2689–2703.
Mul, M.L., Mutiibwa, R.K., Foppen, J.W.A., Uhlenbrook, S., Savenije, H.H.G., 2007. Identification of groundwater flow systems using geological mapping and chemical spring analysis in South Pare Mountains, Tanzania. Phys. Chem. Earth, Parts A/B/C 32 (15–18), 1015–1022.
Mwende BM (2022) Comparative assessment of the impact of land cover change and climate variability on groundwater recharge. IHE Delft Institute for Water Education, Delft, the Netherlands.
Nathan, R.J., McMahon, T.A., 1990. Evaluation of automated techniques for base flow and recession analyses. Water Resour. Res. 26 (7), 1465–1473.
Nonner, J.C., 2002. Introduction to Hydrogeology: UNESCO-IHE Delft Lecture Note Series. CRC Press.
Obando, J.A., Luwesi, C.N., Akombo, R.A., 2024. The impact of land use and cover changes on river flows in Wundanyi Catchment of Taita Hills, Kenya (1970–2030). Sustain. Soc. Develop. 2 (3), 2507.
Oettli, P., Camberlin, P., 2005. Influence of topography on monthly rainfall distribution over East Africa. Climate Res. 28 (3), 199–212.
Oosterom, A.P., 1988. The Geomorphology of southeast Kenya. Wageningen University and Research.
OTT HydroMet (2020) MF Pro operating instructions. DOC026.53.80211, Edition 8.
Palmer, P.I., Wainwright, C.M., Dong, B., Maidment, R.I., Wheeler, K.G., Gedney, N., Hickman, J.E., Madani, N., Folwell, S.S., Abdo, G., Allan, R.P., 2023. Drivers and impacts of Eastern African rainfall variability. Nat. Rev. Earth Environ. 4 (4), 254–270.
Pelletier, A., Andréassian, V., 2020. Hydrograph separation: an impartial parametrisation for an imperfect method. Hydrol. Earth Syst. Sci. 24 (3), 1171–1187.
Pellikka, P.K., Heikinheimo, V., Hietanen, J., Schäfer, E., Siljander, M., Heiskanen, J., 2018. Impact of land cover change on aboveground carbon stocks in Afromontane landscape in Kenya. Appl. Geogr. 94, 178–189.
Pellikka, P.K., Lötjönen, M., Siljander, M., Lens, L., 2009. Airborne remote sensing of spatiotemporal change (1955–2004) in indigenous and exotic forest cover in the Taita Hills, Kenya. Int. J. Appl. Earth Obs. Geoinf. 11, 221–232.
Pettyjohn WA, Henning R (1979) Preliminary estimate of groundwater recharge rates, related streamflow and water quality in Ohio: Ohio State University Water Resources Center Project Completion Report Number 552, p. 323.
Piiroinen R, Heiskanen J, Maeda E, Hurskainen P, Hietanen J, Pellikka PK (2015) Mapping land cover in the Taita Hills, Se Kenya, using airborne laser scanning and imaging spectroscopy data fusion. International Archives of the Photogrammetry, Remote Sensing and Spatial Information Sciences.
Pilgrim DH, Cordery I (1992) Flood runoff. In: Handbook of Hydrology, Ch. 9, New York, McGraw-Hill, pp. 9.1-9.42.
Pohl W, Horkel A, Neubauer W, Niedermayr G, Okelo RE, Wachira JK, Werneck W (1980) Notes on the geology and mineral resources of the Mtito Andei-Taita area (southern Kenya). ÖGG.

Pohl W, Niedermayr G (1979) Geology of the Mwatate Quadrangle [sheet 195/2] and the Vanadium Grossularite Deposits of the Area. Survey, Min., Republic of Kenya.
Ponette-González, A.G., Weathers, K.C., Curran, L.M., 2010. Tropical land-cover change alters biogeochemical inputs to ecosystems in a Mexican montane landscape. Ecol. Appl. 20 (7), 1820–1837.
Prat, O.P., Barros, A.P., 2010. Ground observations to characterize the spatial gradients and vertical structure of orographic precipitation—experiments in the inner region of the Great Smoky Mountains. J. Hydrol. 391, 141–156.
Scanlon, B.R., Healy, R.W., Cook, P.G., 2002. Choosing appropriate techniques for quantifying groundwater recharge. Hydrogeol. J. 10 (1), 18–39.
Somers, L.D., McKenzie, J.M., 2020. A review of groundwater in high mountain environments. Wiley Interdiscip. Rev. Water 7 (6), e1475.
Stuyfzand, P.J., 1989. A new hydrochemical classification of water types. IAHS Publ. 182, 89–98.
Sun, X., Jovanovic, N.Z., Kapangaziwiri, E., Bugan, R.D.H., Brendonck, L., 2013. Application of the rainfall infiltration breakthrough (RIB) model for groundwater recharge estimation in west coastal South Africa. Water SA 39 (2), 221–230.
Svensson, T., Lovett, G.M., Likens, G.E., 2012. Is chloride a conservative ion in forest ecosystems? Biogeochemistry 107 (1), 125–134.
Tuhkanen, S., 1991. The Taita Hills - a verdant mountain massif surrounded by a dry savanna in southeastern Kenya. Land Use Strategies for Survival in the Taita Hills, Taita-Taveta District, Southeastern Kenya. Occasional Papers of the Finnish Association for Development. Geography 25, 203.
Turc, L., 1955. Le bilan d'eau des sols: relations entre les précipitations, l'évaporation et l'écoulement. J. l'hydraulique 3 (1), 36–44.
UN (United Nations), 2025. The United Nations World Water Development Report 2025 - Mountains and glaciers: Water towers. UNESCO, Paris.
University of Helsinki (2024) Forest loss intensifies climate change by increasing temperatures and cloud level, which leads to decrease of water. Available at: https://www.helsinki.fi/en/faculty-science/news/forest-loss-intensifies-climate-change-increasing-temperatures-and-cloud-level-which-leads-decrease-water? (Accessed: 5 March 2026).
van Wyk, E., Van Tonder, G.J., Vermeulen, D., 2012. Characteristics of local groundwater recharge cycles in South African semi-arid hard rock terrains: Rainfall–groundwater interaction. Water SA 38 (5), 747–754.
Vet, R., Artz, R.S., Carou, S., Shaw, M., Ro, C.U., Aas, W., Baker, A., Bowersox, V.C., Dentener, F., Galy-Lacaux, C., Hou, A., Pienaar, J.J., Gillett, R., Forti, M.C., Gromov, S., Hara, H., Khodzher, T., Mahowald, N.M., Nickovic, S., Rao, P.S.P., Reid, N.W., 2014. A global assessment of precipitation chemistry and deposition of sulfur, nitrogen, sea salt, base cations, organic acids, acidity and pH, and phosphorus. Atmos. Environ. 93, 3–100.
Viviroli, D., Dürr, H.H., Messerli, B., Meybeck, M., Weingartner, R., 2007. Mountains of the world, water towers for humanity: typology, mapping, and global significance. Water Resour. Res. 43 (7).
Viviroli, D., Weingartner, R., Messerli, B., 2003. Assessing the hydrological significance of the world's mountains. Mountain Res. Develop. 23 (1), 32–40.
Vogt, N., Wiesenhuetter, J.M., 2000. Pre-feasibility Study, Taita Taveta District, Main Report. 196 p. GTZ / Integrated Food Security Programme – Eastern. Nairobi, Kenya.
Wagner, J., Cook, J., Kimuyu, P., 2019. Household demand for water in rural Kenya. Environ.. Resour. Econ. 74 (4), 1563–1584.
Waswa, G.W., Clulow, A.D., Freese, C., Le Roux, P.A., Lorentz, S.A., 2013. Transient pressure waves in the vadose zone and the rapid water table response. Vadose Zone J.. 12 (1), vzj2012-0054.
Wesely, M.L., Hicks, B.B., 2000. A review of the current status of knowledge on dry deposition. Atmos. Environ. 34 (12-14), 2261-2282.
WHO (World Health Organization), 2017. Guidelines for Drinking-Water Quality, 4th ed. World Health Organization, Geneva.